SYNTHESIS OF SIZE-MODULATED MAGNETITE (Fe$_3$O$_4$) NANOPARTICLES AND ORIGIN OF ITS NEGATIVE CAPACITANCE

A thesis submitted towards partial fulfilment of the requirements for the degree of

Master of Technology in Nanoscience & Technology

Submitted By:

Ankit Dutta

Roll No: M4NST19008

Under the guidance of

Dr. Kalyan Kumar Chattopadhyay

School of Materials Science & Nanotechnology

Jadavpur University

Kolkata- 700032

Courses affiliated to

Faculty Council of Interdisciplinary Studies, Law & Management

Jadavpur University

Kolkata- 700032

2019

Certificate of Recommendation

This is to certify that the thesis entitled "**Synthesis of size-modulated magnetite (Fe$_3$O$_4$) nanoparticles and origin of its negative capacitance**" is a bonafide work carried out by Ankit Dutta under under our supervision and guidance for partial fulfilment of the requirement of Master of Technology in Nanoscience & Technology in School of Materials Science and Nanotechnology during the academic session 2017-19.

_____

Thesis Advisor

Dr. Kalyan Kumar Chattopadhyay

School of Materials Science & Nanotechnology

Jadavpur University,

Kolkata-700032

_____

Dr. Chandan Kumar Ghosh

Director

School of Materials Science & Nanotechnology

Jadavpur University,

Kolkata-700032

_____

Dean

Faculty Council of Interdisciplinary Studies, Law & Management

Jadavpur University

Kolkata- 700032

Certificate of Approval*

This foregoing thesis is hereby approved as a credible study of an engineering subject carried out and presented in a manner satisfactorily to warranty its acceptance as a prerequisite to the degree for which it has been submitted. It is understood that by this approval the undersigned do not endorse or approve any statement made or opinion expressed or conclusion drawn therein but approve the thesis only for purpose for which it has been submitted.

Committee of final examination for

Evaluation of Thesis

_____

_____

_____

_____

*Only in case the thesis is approved

Declaration of Originality & Compliance of Academic Ethics

I hereby declare that this thesis contains literature survey and original research work by the undersigned candidate, as part of his Master of Technology (Nanoscience and Technology) studies during academic session 2017-19.

All information in this document has been obtained and presented in accordance with academic rules and ethical conduct.

I also declare that, as required by this rules and conduct, I have fully cited and referred all material and results that are not original to work.

Name: Ankit Dutta

Roll No: M4NST19008

Thesis Title:

Synthesis of size-modulated magnetite (Fe3O4) nanoparticles and origin of its negative capacitance

_____

Signature   Date:

Acknowledgement:

This work described in the thesis titled "**Synthesis of size-modulated magnetite (Fe$_3$O$_4$) nanoparticles and origin of its negative capacitance**" was initiated in the Thin Film & Nano science Laboratory, Jadavpur University in the year 2017 and would not have been possible without the immense support and invaluable advice from the members of this lab who are nothing less than a large well bonded family.

I could never have reached the heights or explored the depths without the support, guidance and efforts of a lot of people. Prior to everything, I would like to express my earnest gratitude to my project supervisor **Dr. Kalyan Kumar Chattopadhyay** for granting me this opportunity to work under his esteemed guidance in a laboratory that is well equipped with all necessary advanced equipment. His enthusiasm, unlimited support and profound knowledge have been a major learning experience throughout my research work at the Jadavpur University.

I wish to express my sincere thanks to Dr. Chandan Kumar Ghosh, Dr. Mahua Ghosh Chowdhury, Prof. S. Mukherjee, Dr. Sourav Sarkar and Honourable Dean, Faculty of Interdisciplinary Studies, Law & Management for their encouragement during the course.

I would like to express my heartiest thanks to Dr. Nilesh Mazumder and Souvik Bhattacharya for their ideas throughout my project and to make my project successful. Without their guidance, support and immense enthusiasm it would have been impossible for me to complete this project.

I am also thankful to Saikat da, Dimitra di, Antika di, Madhupriya di, Biswajit da, Nripen da, Tufan da and all others for their helpful and supportive nature. My heartiest gratitude to my parents, friends and outstanding labmates Pratik, Debnath, Sumit, Sourav and everyone else for their valuable discussions and constant cooperation throughout the project work.

Date:

_____

Ankit Dutta

Abstract:

Magnetite (Fe_3O_4), a relaxor multiferroic material, has attracted much attention in the last decade due to the recent understandings of charge-ordering phenomena below Verwey transition and uncountable potential biomedical applications. Highly water dispersible spherical Fe_3O_4 nanoparticles (NP's) with enormous variation in size (13 - 236 nm) had been synthesized by a facile solvothermal approach using disodium tartrate and polyethelene glycol as crystal grain growth inhibitor and stabilizer in polyol medium. By controlling the concentration of surfactants, size-distribution of nanoparticles was controlled. Williamson-Hall analysis was employed to evaluate the maximum grain-size of the as-synthesized powder-samples. Average particle-size was also verified from a voigt fit of size-distribution obtained from FE-SEM micrographs, which revealed a close estimation with respect to the W-H grain-size. A thorough XPS analysis was employed to determine the difference in binding energies of the tetrahedral and octahedrally co-ordinated Fe atoms along with degree of stoichiometry and related surface-chemistry. The non-stoichiometry factor (δ) was found independent of particle-size, which resulted a spontaneous non-stoichiometry, common in most multivalent transition metal oxides. In addition, these Fe_3O_4 NP's may be useful in other fields, such as hyperthermia treatment of cancer and targeted drug delivery because of their size-dependent magnetic property and excellent stability.

A persistent low-frequency negative capacitance (NC) dispersion has been detected in half-metallic magnetite (Fe_3O_4) nanoparticles having a size-variation: 13-236 nm; under application of moderate positive DC bias, probed via impedance spectroscopy. A 3D Cole-Cole plot fitting technique has been used employing Harvriliak-Negami model to recapitulate the relaxation time (τ) of the associated oscillating dipoles, related shape-parameters (α,β) and resistivity for different sizes. Universal Debye relaxation (UDR) theory requires a modification to deal with the shifted static NC-dispersion plane in materials showing both +ve and –ve capacitance about a transition-frequency (f_0). A generalized dispersion-formula has been proposed in this regard to fit the complete data of +ve and –ve capacitance regime including the diverging transition-point. In addition, a comprehensive model has been discussed to differentiate the continuous transition from –ve to +ve capacitance due to localized charge recombination and capacitive switching. A consistent blue-shift of 'f_0' was observed with increasing external electric field and decreasing particle-size. An inherent non-stoichiometry due to iron-vacancies [$Fe_{3(1-\delta)}O_4$] detraps holes and builds up p-type nature, which consequently gives rise to more covalent and heavier dipoles slowing down the Maxwell-Wagner interfacial polarization dynamics. This combinational effect has been apprehended for the sluggish response of associated dipoles and stabilization of NC.

Table of Contents

Table of Figures

CHAPTER 1:

INTRODUCTION

1.1   Introduction to Nanoscience & Nanotechnology :

Nanotechnology is science, engineering, and technology conducted at the nanoscale, which is about 1 to 100 nanometers. One nanometer is a billionth of a meter, or 10^{-9} of a meter. Nanotechnology is manipulation of matter on an atomic, molecular, and supramolecular scale. Nanotechnology as defined by size is naturally very broad, including fields of science as diverse as surface science, organic chemistry, molecular biology, semiconductor physics, energy storage, microfabrication, molecular engineering, etc. The associated research and applications are equally diverse, ranging from extensions of conventional device physics to completely new approaches based upon molecular self-assembly, from developing new materials with dimensions on the nanoscale to direct control of matter on the atomic scale.

1.1.1 What is nanotechnology?

Most definitions revolve around the study and control of phenomena and materials at length scales below 100 nm and quite often they make a comparison with a human hair, which is about 80,000 nm wide.

It seems that a size limitation to the 1-100 nm range, the area where size-dependant quantum effects come to bear, would exclude numerous materials and devices, especially in the pharmaceutical area, and some experts caution against a rigid definition based on a sub-100 nm size. This definition reflects the fact that quantum mechanical effects are important at this quantum-realm, and so the definition shifted from a particular technological goal to a research category inclusive of all types of research and technologies that deal with the special properties of matter which occur below the given size threshold. It is therefore common to see the plural form "nanotechnologies" as well as "nanoscale technologies" to refer to the broad range of research and applications whose common trait is size.

Another important criteria for the definition is the requirement that the nano-structure is man-made, i.e. a synthetically produced nanoparticle or nanomaterial. Otherwise we would have to include every naturally formed biomolecule and material particle, in effect redefining much of chemistry and molecular biology as 'nanotechnology'.

1.1.2 How it started?

The ideas and concepts behind nanoscience and nanotechnology started with a talk entitled – "There's Plenty of Room at the Bottom" by physicist Richard Feynman at an American Physical Society meeting at the California Institute of Technology on December 29, 1959; long before the term nanotechnology was used. In his talk, Feynman described a process in which scientists would be able to manipulate and control individual atoms and molecules. Thus, physicist Richard Feynman is called the father of nanotechnology.

1.1.3 Who coined the term Nanotechnology?

The term was coined in 1974 by Norio Taniguchi of Tokyo Science University to describe semiconductor processes such as thin-film deposition that deal with control on the order of nanometres. It wasn't until 1981, with the development of the scanning tunnelling microscope that could "see" individual atoms, with which modern nanotechnology began.

Inspired by Feynman's concepts, K. Eric Drexler used the term "nanotechnology" in his 1986 book "*Engines of Creation: The Coming Era of Nanotechnology"*, which proposed the idea of a nanoscale "assembler" which would be able to build a copy of itself and of other items of arbitrary complexity with atomic control.

Today, scientists and engineers are finding a wide variety of ways to deliberately make materials at the Nano scale to take advantage of their enhanced properties such as higher strength, lighter weight, increased control of light spectrum, and greater chemical reactivity than their larger-scale or bulk counterparts.
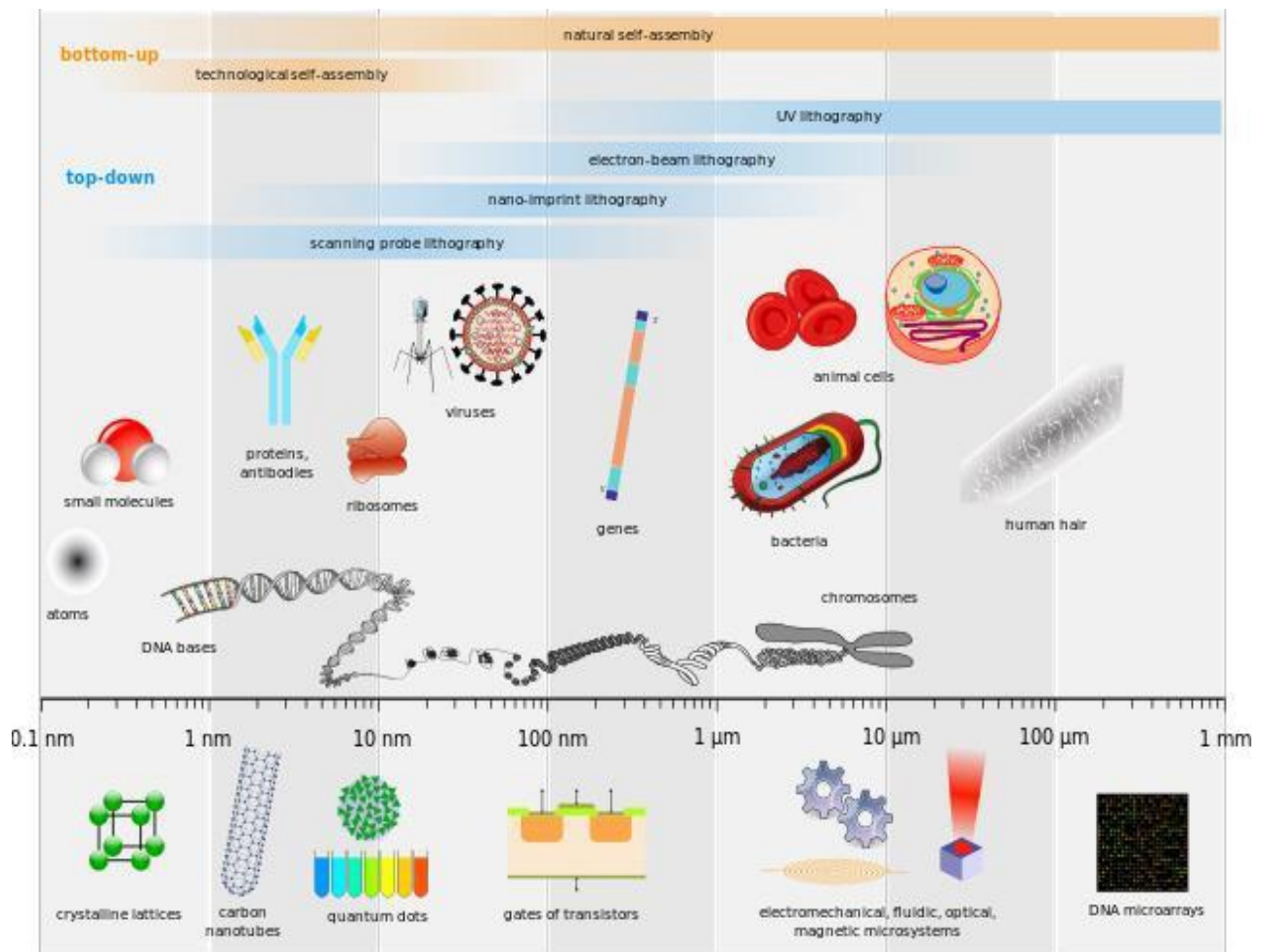
Fig.1.1: Schematic diagram of nanotechnology and its size comparison [1]

1.1.4 A brief history of nanotechnology:

- ❖ **2000 years ago**: Sulphide Nano crystals used by Greeks and Romans to dye hair.

- ❖ **1000 years ago (middle ages):** Gold nanoparticles of different sizes used to produce different colours in stained glass windows

- ❖ **1959:** Physicist Richard Feynman gave a radical lecture at an American Physical

- ❖ Society meeting at Caltech titled – "There's plenty of room at the bottom."

- ❖ **1974: "**Nanotechnology"- Professor Norio Taniguchi for the first time uses the term nanotechnology [4].

- ❖ **1981:** IBM develops Scanning Tunnelling Microscope [5].

- ❖ **1985: "**Bucky ball"- Scientists at Rice University and University of Sussex discover Fullerene (C60) [6].

- ❖ **1986:** "Engines of Creation"– First book on nanotechnology by K. Eric Drexler [7]. Atomic Force Microscope invented by Binnig, Quate, and Gerbe.

- ❖ **1989:** IBM logo made with individual atoms.

- ❖ **1991:** Carbon Nanotubes discovered by S. Ijima.

- ❖ **1999:** "Nano medicine"– First Nano medicine book by R. Freitas.

- ❖ **2000:** "National Nanotechnology Initiative" was launched.

1.1.5 What distinguishes nanomaterial from bulk?

- ❖ While most micro structured materials have similar properties to the corresponding bulk materials, the properties of materials with nanometre dimensions are significantly different from those of atoms and bulk materials. Among the characteristics of nanomaterial that distinguish them from bulk materials, it is important to note the following:

- ❖ Large fraction of surface atoms;

- ❖ High surface energy;

- ❖ Spatial confinement

- ❖ Reduced numbers of imperfections that do not exist in the corresponding bulk materials [1].

The use of nanomaterial provides the following advantages [1].

First, all nanomaterial consist of very small particles. This is the first advantage of nanomaterial and nanotechnologies, promoting attainment of super miniaturization. Because they are small, nanostructures can be packed very closely together. As a result, on a given unit of area one can locate more functional Nano devices, which is very important for Nano electronics. Their high packing density has the potential to bring higher area and volume

capacity to information storage and higher speed to information processing (because electrons require much less time to move between components). Thus, new electronic device concepts, smaller and faster circuits, more sophisticated functions, and greatly reduced power consumption can all be achieved simultaneously by controlling nanostructure interactions and complexity.

Second, because of their small dimensions, nanomaterials have large specific surface areas, accelerating interactions between them and the environment in which they are located. Nanoparticles have a much larger surface area per unit of mass compared with larger particles. Because growth and catalytic chemical reactions occur at surfaces, this means that materials in nanoparticle form will be much more reactive than the same mass of material made up of larger particles. A strong increase in the participation of surface atoms in the physical and chemical properties of nanomaterials is another consequence of a decrease in particle size.

It is known that the volume of an object decreases as the third power of its linear dimensions, but the surface area decreases only as its second power. In case of nanoparticles, the surface area-to-volume ratio (the ratio between surface and bulk atoms) increases than that of bulk. The variation of surface or volume ratio as a function of particle size is given in Fig.1.3
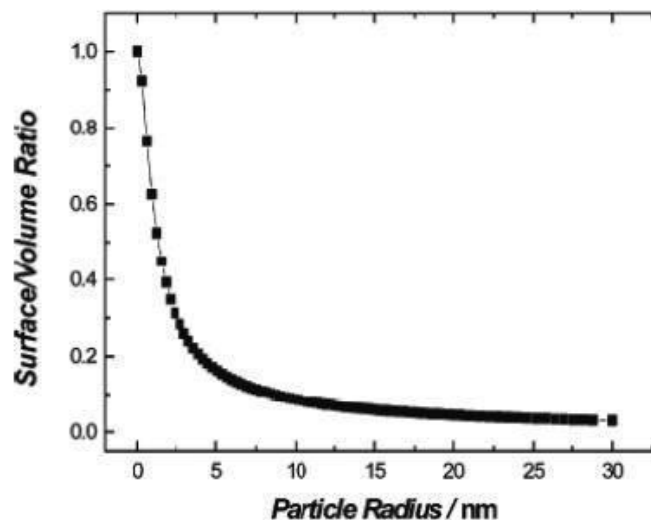
Fig.1.2: Surface/volume ratio as a function of particle size [8]

It is known that atoms on the surface of nanoparticles have unusual properties. These surface atoms make nanoparticles very different from just small particles, because not all bonds of surface atoms with neighbouring atoms are enabled. For atoms on uneven surfaces, no

saturation of the bonds is even higher. For this reason, corner atoms normally have the highest affinity to form bonds to adsorbate molecules, followed by edge and in-plane surface atoms, a fact that is of great importance for catalytic activity. Alternatively, because of their low stabilization due to low coordination, edge and in particular corner atoms are often missing on single crystals, even in thermodynamic equilibrium [9]. Recently, size-dependent variation in oxidation state and lattice parameter has been reported for cerium oxide nanoparticles [10].

As a result of the changes that occur in particles with a decrease of particle size, nanomaterials can have extremely high biological and chemical reactivity. For example, catalytically active nanomaterials allow accelerating either chemical or biochemical reactions by tens of thousands, and even a million times. This attribute explains even 1 g of nanomaterial can be more effective than 1 ton of a similar but macro substance.

Another aspect we must consider is that the free surface is a place of accumulation (sink) of crystallographic defects. At small particles sizes, the surface concentration of such defects increases considerably. Hardeveld and Hartog in 1969 calculated classically and showed that the largest changes of proportions between facets, edges, corners, and micro defects at the surface occur between 1 and 5 nm [11]. As a result, strong lattice distortion and even a change of lattice type can take place on the surface layer. In fact, due to accumulation of structural defects and chemical impurities on the surface, we can observe purification of the bulk area of the nanoparticles.

An important specific characteristic of nanomaterial properties (we mean here polycrystalline materials with grain size less than 40 nm) is an increase of the role of interfaces with decrease of the size of grains or crystallites in nanomaterials. Experimental research has shown that the state of grain boundaries has a non-equilibrium character, conditioned by the presence of the high concentration of grain boundary defects. This non equilibrium is characterized by extra energy of the grain boundaries and by the presence of long-range elastic stress. At the same time, the grains have ordered crystallographic structure, while the grain boundary defects act as a source of elastic strains. Non-equilibrium of the grain boundaries initiates the occurrence of the lattice distortion, the change of interatomic distances, and the appearance of sufficient displacement of atoms, right up to loss of an ordered state.

Another important factor peculiar to nanoparticles is their tendency to aggregation. The possibility of migration (diffusion) of either atoms or groups of atoms along the surface and the boundaries, as well as the presence of attractive forces between them, often leads to processes of self-organization into various cluster structures. This effect has already been used for creation of ordered nanostructures in optics and electronics.

One more important aspect of nanomaterial properties is connected with the fact that, during transport processes (diffusion, electro- and thermal conductivity, etc.), there are certain effective lengths of free path of a carrier of this transport (L_e), such as phonon and electron mean free paths, the Debye length, and the excition diffusion length for certain polymers. While proceeding to sizes smaller than L_e, transport speed starts to depend on both the size and the shape of the nanomaterial; generally, the transport speed increases sharply [12].

The principal characteristics of nanomaterials are conditioned by not only by their small the size, but also by the appearance of new quantum mechanical effects in a dominating role at the interface (Esaki 1991 [13]; Serena and Garcia 1997 [14]). Those quantum size effects occur at a critical size, which is proportionate with the so-called correlative radius of one or another physical phenomena, for example, with the length of the free path of electrons or photons, the length of coherence in a superconductor, sizes of magnetic domains, and so on. As a rule, quantum size effects appear in materials with crystallite sizes in the nano range D <10 nm. As a result, in nanomaterials with characteristic size, one can expect the appearance of effects which cannot be observed in bulk materials.

1.1.6 Classification of Nanomaterials:

Zero dimension< 100nm	**Particles, quantum dots, hollow Spheres, etc.**
One dimension < 100nm	Nanorods, nanowires etc.
Two dimensions < 100nm	Tubes, fibres, platelets, etc.

[1] Fig 1.3:Categories of Nanomaterials

Nanomaterials can be classified dimension wise into following categories shown in Fig 1.3

On the basis of phase composition, nanomaterials in different phases can be classified as,

- ❖ Single phase solids include crystalline, amorphous particles and layers, etc.
- ❖ Multi-phase solids include matrix composites, coated particles, etc.
- ❖ Multi-phase systems include colloids, aero gels, Ferro fluids, etc.

1.1.7 Synthesis of Nanomaterials:

In order to explore the unique physical properties & phenomena and also to realize the useful applications of nanostructures and nanomaterial, the ability to fabricate and process nanomaterial and nanostructures is the first hurdle in nanotechnology. The following schematic diagram in Fig. 1.4 shows the two significant approaches in the synthesis of nanomaterial.
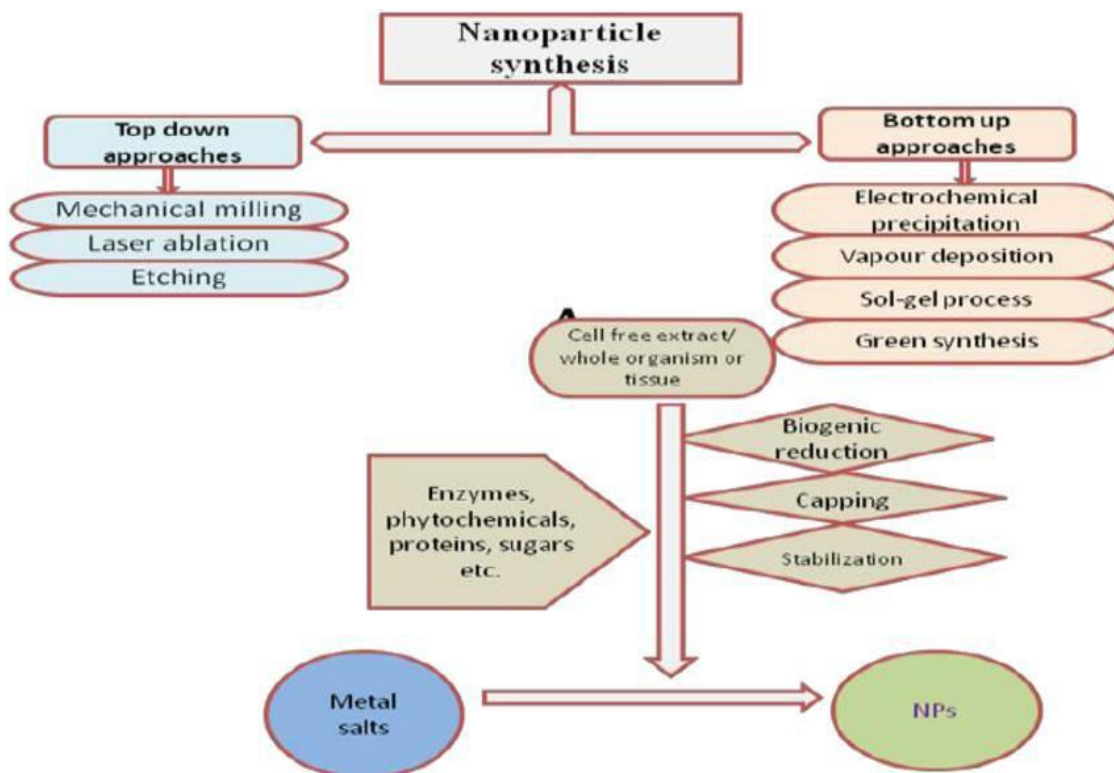
Fig.1.4: Schematic diagram of different synthesis approaches of nanomaterial

For the fabrication and processing of nanomaterial and nanostructures, the following challenges must be taken care of [1]:

- ❖ Overcome the huge surface energy, a result of enormous surface area or large surface-to- volume ratio.
- ❖ Ensure all nanomaterial with desired size, uniform size distribution, morphology, crystallinity, chemical composition, and microstructure which result in desired physical properties.

❖ Prevent nanomaterial and nanostructures from coarsening through either Ostwald ripening or agglomeration.

Many technologies have been explored to fabricate nanostructures and nanomaterial. These technical approaches can be grouped in several ways like growth media or the form of products.

1. According to growth media:

a. Vapour phase growth, including laser reaction pyrolysis for nanoparticle synthesis and atomic layer deposition (ALD) for thin film deposition.
b. Liquid phase growth, including colloidal processing for the formation of nanoparticles and self-assembly of monolayers.
c. Solid phase formation, including phase segregation to make metallic particles in glass matrix.

2. According to the form of products:

a. Nanoparticles by means of colloidal processing, flame combustion and phase segregation.
b. Nano rods or nanowires by template-based electroplating, solution liquid- solid growth (SLS), and spontaneous anisotropic growth.
c. Thin films by molecular beam epitaxy (MBE) and atomic layer deposition (ALD).

3. 'Top Down' and 'Bottom Up Approach':

The top down approach uses traditional methods to guide the synthesis of Nano scale materials [1, 15]. The paradigm proper of its definition generally dictates that in the top down approach it all begins from a bulk piece of material, which is then gradually or step by step removed to form objects in the nanometre-size regime. Well known techniques such as photo lithography and electron beam lithography, anodization, ion and plasma etching all belong to this type of approach. The bottom up approach is exactly the opposite of top down approach. In this case instead of starting with large materials and chipping it away to reveal small bits of it, it all begins from atoms and molecules that get rearranged and assembled to large nanostructures. It is the new paradigm for synthesis in the nanotechnology world as the

bottom up approach allows a creation of diverse types of nanomaterial, and it is likely revolutionize the way of material fabrication. Schematic representation of Bottom up and Top down approach is shown in Fig.1.5.
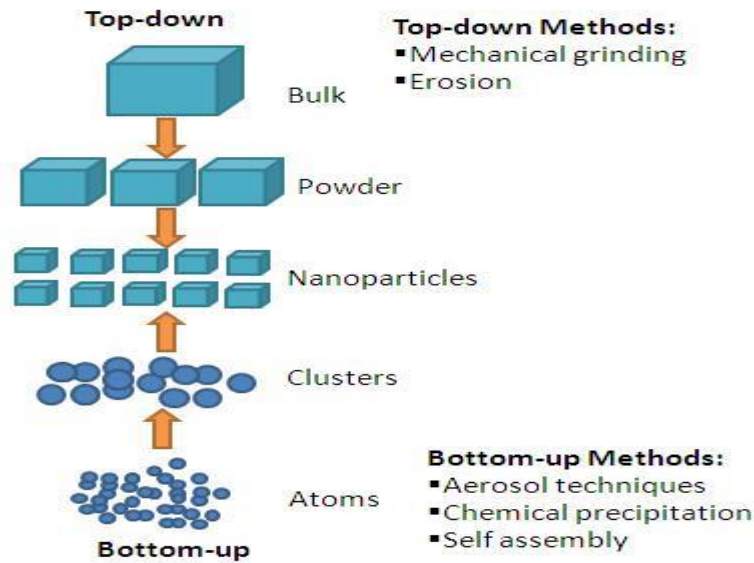
Fig.1.5: Schematic diagram of Top Down and Bottom Up Approach

Attrition or Milling is a typical top down method in making nano particles, whereas the colloidal dispersion is a good example of bottom up approach in the synthesis of nano particles.

4. Self-assembly:

One bottom-up method is nature's way; — *"self-assembly"*. Self-organizing processes are common throughout nature and involve components from the molecular (e.g. protein folding) to the planetary scale (e.g. weather systems) and even beyond (e.g. galaxies). The key to using self-assembly as a controlled and directed fabrication process lies in designing the components that are required to self-assemble into desired patterns and functions. Selfassembly reflects information coded- as shape, surface properties, charge, polarizability, magnetic dipole, mass etc. in individual components; these characteristics determine the interactions among them [16].

1.1.8 Applications of Nanotechnology:

Nano technological application is extended in different field of research with various unique applications. When a particle is shrunk to nano-scale, several properties of the material change in accordance with size. So it gives new applications in several fields. As due to the size the surface to volume ratio increases, it gives more surface area to react. Several optical as well as mechanical properties are also dependent on the diameter or the size of particles. The following diagram of **Fig.1.6** shows some few such applications.
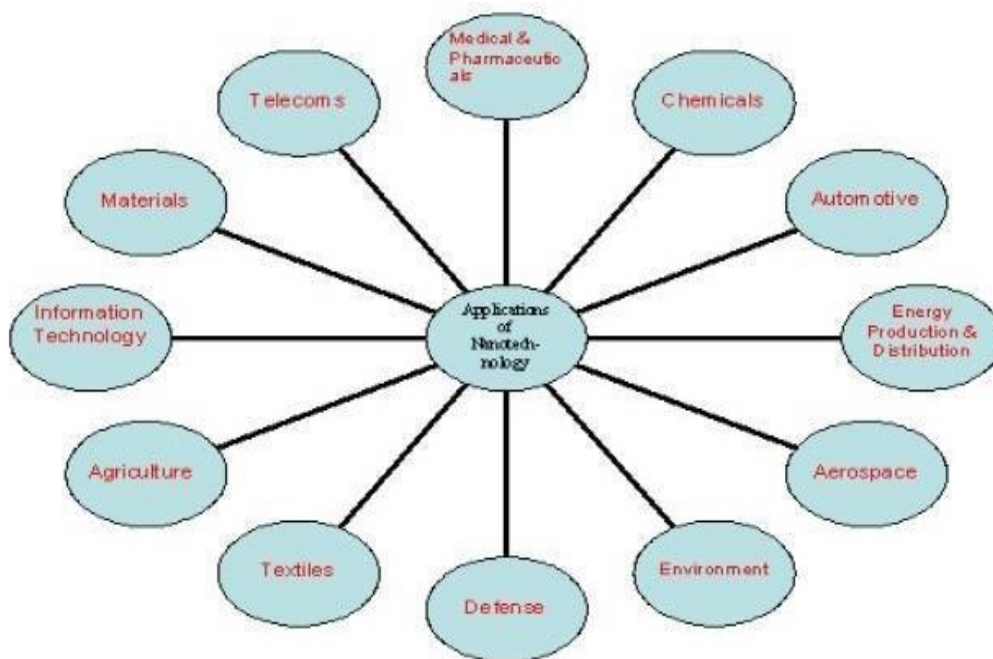
Fig.1.6: Applications of Nanotechnology

Nanotechnology has innumerable applications in variety of diverse fields all of which are interconnected with each other. The modern world has burgeoned in a consequential extent with the advent of newer technologies based on Nano science [17]. The applications include nanoscale pattering of electronic circuits, high density data storage, quantum computers, fuel cell catalysts, environmental catalysts, industrial catalysts, waste water treatment, functional nanocomposites, food packaging, food processing catalysts, hydrogen production photocatalysts, automotive catalysts, fuel additive catalysts, lithium ion battery electrodes, natural or synthetic polymer hybrid fibres, reinforced plastics, controlled drug release, cancer therapy, drug delivery, bio imaging, bio markers, hyperthermic treatment, MRI contrast agents, IR contrast agents, ultra violet protection like sunscreens, antioxidants, ultra violet blocking coatings, water resistant coatings, gas barrier coatings, anti-microbial coatings, self-

cleaning building surface, food quality and safety analysis sensors, chemical sensors, gas sensors, high sensitive sensors, pollution monitoring sensors, functional nanocomposites, nano pigments, super thermal-conductive liquid, nano phosphors for display, super plastic ceramics, transparent conductive polymer films, chemical mechanical planarization, nano inks, single electron transistors, quantum lasers, high power magnets, pollutant scavengers, interactive food, neutraceutical, fungicides and pesticides, medical textiles, technical textiles, heat retaining textiles, self-cleaning textiles, anti-stain textiles, electro-conducting textiles, ultra violet blocking textiles, wound dressing, dental ceramics, bone growth, tissue cells engineering, molecular tagging, dye sensitized solar cells, paint-on solar cells, hydrogen storage materials, bio-composites, Ferro-fluids, refractive index engineering, aerospace engineering and many others. Detail applications in some important fields are given below:

❖ **Nanotechnology in Energy and Environment:**

is basically the extension of microelectronics and research in Nano electronics will develop CNT, Graphene based flexible independent electronic devices in future.

1. CNT based field emission display is highly efficient because light weight CNT can be used as field emitters with extremely high efficiency for field emission displays (FED) with very low power consumption.

2. Nanotechnology is employed to increase the density of memory chips. Researchers are developing a type of memory chip with a projected density of one terabyte of memory per square inch or greater. Integrated nanosensors are used for collecting, processing and communicating massive amounts of data with minimal size, weight, and power consumption.

3. Research in nanotechnology introduces transistors with Graphene and CNT as active materials and CNT transistor based processor for computer application is about to commercialize in future market. Due to their smaller size and lower power consumption CNT and Graphene based transistors are easy to integrate in the integrated circuits.

4. Large magnetic moment and adequate coercivity nanomaterial can help to produce magneto caloric effect on a particular scale so that refrigeration could be possible without need of refrigeration fluids.

5. Solid state lightening is a powerful tool to reduce total electricity consumption by 10% and cut carbon emission by the equivalent of 28 million tons/year.

❖ **Nanotechnology in Flexible Electronics:**

Nanotechnology in electronic industry is gradually becoming popular because smaller size and compact design of electronic devices can ensure faster processing, reduction of delay in circuitry and processing power consumption. Nanotechnology in electronics industry introduces microprocessors less than 100 nanometres (nm) in size. However, Nanoelectronics is basically the extension of microelectronics and research in Nano electronics will develop CNT, Graphene based flexible independent electronic devices in future.

1. CNT based field emission display is highly efficient because light weight CNT can be used as field emitters with extremely high efficiency for field emission displays (FED) with very low power consumption.

2. Nanotechnology is employed to increase the density of memory chips. Researchers are developing a type of memory chip with a projected density of one terabyte of memory per square inch or greater. Integrated nanosensors are used for collecting, processing and communicating massive amounts of data with minimal size, weight, and power consumption.

3. Research in nanotechnology introduces transistors with Graphene and CNT as active materials and CNT transistor based processor for computer application is about to commercialize in future market. Due to their smaller size and lower power consumption CNT and Graphene based transistors are easy to integrate in the integrated circuits.

4. Large magnetic moment and adequate coercivity nanomaterial can help to produce magneto caloric effect on a particular scale so that refrigeration could be possible without need of refrigeration fluids.

❖ **Nanotechnology in Health and Medicine:**

Nanotechnology has a high impact on the research and applications related to biology and medicine. Nano-drug delivery is the safest procedure for medication because small quantity of nanomaterial can help to recover with reducing side effects. Nano medicine has also the potential to enable early detection and prevention, and to essentially improve diagnosis, treatment and follow-up of diseases with the help of bio-sensors.

1. Carbon nanotubes have promising application for the development of advanced biosensors with novel features CNT, though inert, can be functionalized at the tip with a probe molecule. Their study uses AFM as an experimental platform. i. Leukaemia cells identification

2. Catheter development.

3. Nano devices can make gene sequencing more efficient.

4. Tissue engineering makes use of artificially stimulated cell which can help in transplantation of organs or artificial implants.

5. The technology is also being used to develop sensors for cancer diagnostics.

❖ **Nanotechnology in Transportation:**

Nanomaterial is used as faster and cost effective new fuel source. The main advantage of using nanomaterial is light weight so that easy to carry in fuel chamber of cars and aeroplanes.

1. Suitable Nanomaterials can effectively reduce the emission of pollutants in the process of incomplete combustion in engine. Nano Twin Technologies has recently released an air filter to remove hazardous chemicals from the air in car cabins.

2. Nanoparticles of inorganic clays and polymers are an effective alternative for carbon black tires results in environmental friendly, wear resistant tires. Frictional resistant tires are also made possible through Nano science.

3. Nano coating of metallic surfaces such as steel to achieve super-hardening, low friction, and enhanced corrosion protection.

❖ **Nanotechnology in Defence and Security:**

Nanotechnology will lead to higher protection, more lethality, longer endurance and better self-supporting capacities of future combat soldiers. Substantial advantages are expected to be gained which include threat detection, novel electronic display and interface systems, as well as a pivotal role for the development of miniaturised unmanned combat vehicles and robotics. Nanotechnology will also enable small portable sensor systems capable of identifying chemical, biological and nuclear, radiation, or explosive threats.

❖ **Nanotechnology in Information & Communication:**

Electronic memory designs in the past have largely relied on the formation of transistors. The miniaturization of electronic industry has been the driving force behind the rapid research and development of Nano science and technology. Continuing to shrink silicon chips is getting expensive and difficult. Chips built using the molecular transistors are the industry's best hope for building faster, cheaper computers well into this century. "With the electronics we're talking about, we're going to make a computer that doesn't just fit in your wristwatch, not just in a button on your shirt, but in one of the fibres of your shirt," says Philip Kuekes, a

computer architect at Hewlett-Packard Laboratories. According to the manufacturers, NRAM (Nanotube-based/Non-volatile random access memory) is a universal memory chip suitable for countless existing and new applications in the field of electronics. In the modern communication technology traditional analog electrical devices are increasingly replaced by optical or optoelectronic devices due to their enormous bandwidth and capacity. Two promising examples are photonic crystals and quantum dots. Quantum dots are nanoscale objects, which can be used for the construction of lasers. The advantage of a quantum dot laser over the traditional semiconductor laser is that their emitted wavelength depends on the diameter of the dot. Quantum dot lasers are cheaper and offer a higher beam quality than conventional laser diodes.

❖ **Nanotechnology in Filtration:**

Nanoporous membranes are suitable for filtration with extremely small pores like 10nm. It is mainly used for separation of ions or different fluids which find application in renal dialysis. Nanoscale particles increase the efficiency of absorbing contaminants and it is relatively inexpensive compared to traditional filtration methods.

1.2 Introduction to Negative Capacitance

1.2.1 Brief description of negative capacitance phenomena

A capacitor is a device that consists of two metallic electrodes separated by a dielectric material. When external bias is applied to electrodes, the dielectric inside the capacitor gets polarized. If, upon the application of external bias across a nonlinear conductor, significant minority carrier generation takes place along with regular majority carrier generation, the resultant capacitance of the dielectric may take a negative value. Negative capacitance generation has been mainly attributed to the presence of significant minority carrier concentration.

Zinc oxide is a prototype *n*-type semiconductor with wide indirect optical gap of around 3 eV. As ZnO is an *n*-type semiconductor, the majority carriers are electrons. From previous investigation carried out on the negative capacitance in ZnO, it was observed that if chalcogen elements (S, Se and Te) are doped substitutionally at O-site of ZnO lattice, the

attractor capacity weakens between electrons and holes gradually from ZnO to ZnO/Te, the tendency of delocalization increases for the electron cloud, which as a consequence prompts the bound holes also to be delocalized. Thus, hole generation occurs which is minority carrier

in ZnO and thus gradual generation of holes result in negative capacitance upon the application of a threshold external bias.

1.2.2 Overcoming 'Boltzmann Limit' by negative capacitance effect

The Boltzmann distribution of electrons possesses a fundamental barrier to lowering energy dissipation in conventional electronics, often termed as Boltzmann Tyranny. Many scientists believe that the fundamental limits on the minimum operational voltage and switching energy of transistors is given by the "Boltzmann tyranny' argument."

Negative capacitance has importance regarding transistor miniaturization. This is because simple constant-electric-field scaling rules had guided the shrinking of field-effect transistors (FETs). As transistors shrank, they switched faster and used less power to switch. But constant-field scaling requires that operating voltages decrease in tandem with transistor dimensions. In recent years, this has become increasingly difficult to follow because a minimum gate voltage swing is necessary to switch the device from a — 'off' (low-current) state to a — 'on' (high-current) state. If that swing is too small, the device designer is faced with two bad choices: excessive leakage current in the nominally —'off' state or low current (slow circuits) in the nominally — 'on' state. Thus, over the past 10 years, the industry gradually moved from constant-field scaling towards constant voltage scaling. Companies continue to shrink the transistor, emphasizing the increasing number of parallel processors (cores) they can place on a single silicon chip. The only way to decisively break the power dissipation bottleneck is to change the physics of transistor operation in ways that facilitate further reduction of operating voltage. That means increasing the non-linearity of the switching behaviour so that a much smaller swing in gate voltage is needed to switch the device from off to on.

Complementary metal-oxide-semiconductor (CMOS) scaling is facing a fundamental barrier stemming from the Boltzmann statistics which dictate that a minimum voltage must be applied to affect an order of magnitude increase in the current. This means that CMOS voltage and transistor power dissipation cannot be downscaled arbitrarily. Therefore, it has

been suggested that without introducing fundamentally new physics in transistor operation, an end to scaling is inevitable. In that pursuit, it was proposed that the minimum voltage requirement could be overcome if the ordinary gate oxide could be replaced by another stack that provides an effective negative capacitance (NC). The key to overcoming the Boltzmann limit by negative capacitance lies in the fact that, in a series combination of a negative and a positive capacitor, the total capacitance becomes larger than its constituent positive capacitor. Notably, this is just the opposite of what happens in a classical series combination of two positive capacitors, where the total capacitance is always reduced. For a MOSFET, a negative gate capacitance can make the total capacitance, looking into the gate, larger than the semiconductor capacitance. To induce the same amount of charge in the channel, one would require a smaller voltage than what would be required classically. This, in turn, means that the gate voltage could be reduced below the classical limit.

The concept of ferroelectrics displaying effective negative permittivity has led to the speculation that its inclusion in the gate stack of a metal oxide semiconductor field effect transistor (MOSFET) will reduce the sub threshold swing of complementary metal oxide semiconductor (CMOS) devices below 60 mV/dec.[1] For a gate stack comprising a thin ferroelectric layer on top of a thin insulator layer, the channel potential (Ψs) can change more than the gate voltage (Vg) thus providing a step-up voltage transformer and S < 60 mV/dec. If this can be engineered, it heralds a transformation of future integrated circuits (ICs), reducing the off-state current (I_{off}) and/or supply voltage (VDD) that otherwise limits Moore's Law as heat generated during switching cannot be removed. The idea has led to the search for unambiguous experimental evidence of negative capacitance in candidate ferroelectrics at room temperature as a step toward this ambition.

Ferroelectric materials display spontaneous electric polarization, which can be aligned by an applied electric field. Negative capacitance can be measured in ferroelectric materials. But for one thing, the ferroelectric 'negative capacitance state' is intrinsically unstable because it exists only around the tipping point between the two thermodynamically stable polarization states.

1.3 Objective:

The primary objective of this thesis is to investigate the negative capacitance dispersion in chalcogen doped and lithium sulphur co-doped zinc oxide. In the first part of the work, effect of *Ch* doping at O-site in ZnO on the bias dependent NC dispersion is investigated along with the analysis of other dynamical parameters like electric susceptance, conductance, impedance phase angle and admittance phase angle. In the second part, Li and (Li+S) doping is carried out in ZnO for observing the effect of site selective hole generation on NC dispersion. Systematic correlation of the experimental outcome could have a transformative impact in a broad range of devices that may operate at lower frequency and must operate with low power levels as ZnO is CMOS compatible material. Here, our primary purpose is to achieve NC dispersion at a very low voltage threshold (mV) to deal with the excess power dissipation problem in nanoscale devices. Generally, household appliances work in 220V but we want to lower the bias threshold to 8 V at least for electronic applications like mobiles, computers, laptops etc.

Negative capacitance can also provide voltage amplification for low power nanoscale devices. Negative capacitance could bring more efficient transistors. The goal in making transistors with negative capacitance is to make more efficient transistors that consume less power, especially for power-constrained applications such as mobile phones, distributed sensors, and emerging components for the internet of things.

The most difficult problem in nano-electronics is the management of the heat generated during information processing. However, heat removal from semiconductor devices is fundamentally difficult today, and could become a nightmare tomorrow. So to remove that heat we need to ‗generate less heat and/or remove it more effectively' but, in reality, both these options are very problematic. The self-heating that occurs in transistors can be reduced by the heat dissipation property of negative capacitance.

Negative capacitance is important regarding transistor miniaturization. Transistors are becoming too small and clock speed too fast to reduce the heat generated during switching, resulting in increased power dissipation and overheating. Because the dissipated power is proportional to the square of the voltage, a potential solution is to reduce the voltage applied. Negative capacitance generation can be generated in metal oxides which are ferroelectric and CMOS compatible. ZnO is a ferroelectric metal oxide.

1.4 References :

1. Nanostructures and Nanomaterials: Synthesis, Properties and Applications; Guozhong Cao.

2. Introduction to Nanoscience, Kai Nordlund; 2005.

3. Iijima, S., 1991; Helical microtubules of graphitic carbon. N*ature*, *354*(6348), pp.56- 58.

4. N. Taniguchi, "On the Basic Concept of 'Nano-Technology'," Proc. Intl. Conf. Prod. Eng. Tokyo, Part II, Japan Society of Precision Engineering, 1974.

5. G. Binnig et al., Phys. Rev. Lett. 49, 57,(1982).

6. Smalley, R.E., 1997. Discovering the fullerenes. *Reviews of Modern Physics*, *69*(3), p.723.

7. K.E. Drexler, Engines of creation: The coming era of nanotechnology, (Oxford University Press, Oxford, 1986); K.E. Drexler, C. Terson, G. Pergamit, Unbounding the Future: The Nanotechnology Revolution (Morrow, New York, 1991); K.E. Drexler, Nanosystems: Molecular Machinery, Manufacturing, and Computation,(Wiley, New York, 1992).

8. Burda, C., Chen, X., Narayanan, R. and El-Sayed, M.A., 2005. Chemistry and properties of nanocrystals of different shapes. *Chemical reviews*, *105*(4), pp.1025-1102.

9. Roduner, E., 2006. Size matters: why nanomaterials are different. *Chemical Society Reviews*, *35*(7), pp.583-592.

10. Deshpande, S., Patil, S., Kuchibhatla, S.V. and Seal, S., 2005. Size dependency variation in lattice parameter and valency states in nanocrystalline cerium oxide. *Applied Physics Letters*, *87*(13), pp.133113-133113.

11. Van Hardeveld, R. and Hartog, F., 1969. The statistics of surface atoms and surface sites on metal crystals. *Surface Science*, *15*(2), pp.189-230.

12. Law, M., Goldberger, J. and Yang, P., 2004. Semiconductor nanowires and nanotubes.

13. Tsu, R. and Esaki, L., 1991. Stark quantization in superlattices. *Physical Review B*, *43*(6), p.5204.

14. Costa-Krämer, J.L., García, N., García-Mochales, P., Serena, P.A., Marqués, M.I. and Correia, A., 1997. Conductance quantization in nanowires formed between micro and macroscopic metallic electrodes. *Physical Review B*, *55*(8), p.5416.

15. C.N. chinthamani nagesa ramachandra rao, P.john Thomas, G.U. kulkarni, Nano crystal: synthesis, properties and applications, (2007).

16. Shimizu, T. ed., 2008. *Self-assembled nanomaterials II: Nanotubes* (Vol. 220). Springer.

17. http://www.nanowerk.com/nanotechnology-applications.php

18. Montigaud, H., Tanguy, B., Demazeau, G., Alves, I. and Courjault, S., 2000. C3N4: Dream or reality? Solvothermal synthesis as macroscopic samples of the C3N4 graphitic form. Journal of materials science, 35(10), pp.2547-2552.

19. Y. Gu, L. Chen, L. Shi, J. Ma, Z. Yang and Y. Qian, Carbon, 2003, 41, 2674.

20. Q. Guo, Y. Xie, X. Wang, S. Zhang, T. Hou and S. Lv, Chem. Commun., 2004,

21. Ying Zhou; et al. (2008). "Hydrothermal synthesis of ZnO nanorod arrays with the addition of polyethyleneimine". Materials Research Bulletin. 43 (8–9): 2113–2118.

22. Takahashi, Kiyoshi; Yoshikawa, Akihiko; Sandhu, Adarsh (2007). Wide bandgap semiconductors: fundamental properties and modern photonic and electronic devices.

23. Ohgaki, Takeshi; Ohashi, Naoki; Sugimura, Shigeaki; Ryoken, Haruki; Sakaguchi, Isao; Adachi, Yutaka; Haneda, Hajime (2008). "Positive Hall coefficients obtained from contact misplacement on evident n-type ZnO films and crystals". Journal of Materials Research.

24. Ryu, Y. R.; Lee, T. S.; White, H. W. (2003). "Properties of arsenic-doped p-type ZnO grown by hybrid beam deposition". Applied Physics Letters. 83: 87.

25. Tien, L. C.; Sadik, P. W.; Norton, D. P.; Voss, L. F.; Pearton, S. J.; Wang, H. T.; Kang, B. S.; Ren, F.; Jun, J.; et al. (2005). "Hydrogen sensing at room temperature with Pt-coated ZnO thin films and nanorods". Applied Physics Letters. 87 (22): 222106

26. Nav Bharat Metallic Oxide Industries Pvt. Limited. Applications of ZnO. Archived February 26, 2009, at the Wayback Machine. Access date January 25, 2009.

27. https://www.nano.gov/nanotech-101/what/definition

28. https://www.nanowerk.com/nanotechnology/introduction/introduction_to_nanotechnology_1.php

29. Zhang, Z., Leinenweber, K., Bauer, M., Garvie, L.A., McMillan, P.F. and Wolf, G.H., 2001. High-Pressure Bulk Synthesis of Crystalline C6N9H3⊙ HCl: A Novel C3N4 Graphitic Derivative. Journal of the American Chemical Society, 123(32), pp.7788-7796.

30. Guo, Q., Xie, Y., Wang, X., Lv, S., Hou, T. and Liu, X., 2003. Characterization of well-crystallized graphitic carbon nitride nanocrystallites via a benzene-thermal route at low temperatures. Chemical Physics Letters,380(1), pp.84-87.

31. 18. Liebig, J., 1834. Uber einige Stickstoff-Verbindungen. Annalen der Pharmacie, 10(1), pp.1-47.

32. Franklin, E.C., 1922. The ammono carbonic acids. Journal of the American Chemical Society, 44(3), pp.486-509.

33. Redemann, C.E. and Lucas, H.J., 1940. Some derivatives of cyameluric acid and probable structures of melam, melem and melon. Journal of the American Chemical Society, 62(4), pp.842-846.

34. Jürgens, B., Irran, E., Senker, J., Kroll, P., Müller, H. and Schnick, W., 2003. Melem (2, 5, 8-triamino-tri-s-triazine), an important intermediate during condensation of melamine rings to graphitic carbon nitride: Synthesis, structure determination by X-ray powder diffractometry, solid-state NMR, and theoretical studies. Journal of the American Chemical Society, 125(34), pp.10288-10300.

35. Lotsch, B.V., Döblinger, M., Sehnert, J., Seyfarth, L., Senker, J., Oeckler, O. and Schnick, W., 2007. Unmasking Melon by a Complementary Approach Employing Electron Diffraction, Solid-State NMR Spectroscopy, and Theoretical Calculations—Structural Characterization of a Carbon Nitride Polymer. Chemistry–A European Journal, 13(17), pp.4969-4980.

36. Niu, C., Lu, Y.Z. and Lieber, C.M., 1993. Experimental realization of the covalent solid carbon nitride. Science, 261(5119), pp.334-337.

37. Bai, X.D., Zhong, D., Zhang, G.Y., Ma, X.C., Liu, S., Wang, E.G., Chen, Y. and Shaw, D.T., 2001. Hydrogen storage in carbon nitride nanobells. Applied Physics Letters, 79(10), pp.1552-1554.

38. Kouvetakis, J., Todd, M., Wilkens, B., Bandari, A. and Cave, N., 1994. Novel synthetic routes to carbon-nitrogen thin films. Chemistry of materials,6(6), pp.811-814.

39. https://en.wikipedia.org/wiki/Nanotechnology

40. Emil Venere. 'Negative capacitance' could bring more efficient transistors

41. Zhao, Y.C., Yu, D.L., Zhou, H.W., Tian, Y.J. and Yanagisawa, O., 2005. Turbostratic carbon nitride prepared by pyrolysis of melamine. Journal of materials science, 40(9), pp.2645-2647.

42. Tro, Nivaldo J. Chemistry: A Molecular Approach. Upper Saddle River: Pearson Education, 2008. Print. (379-386)

43. Mazumder.N, Mandal.P, Roy.R, Ghorai.U.K., Saha. S, and Chattopadhyay.K.K . Negative capacitance in $ZnO_{1-x}Ch_x$ (Ch = S, Se, Te): Role of localized charge recombination. Journal of Applied Physics 121, 135702 (2017)

44. Mengwei Si, Chun-Jung Su, Chunsheng Jiang, Nathan J. Conrad, Hong Zhou, Kerry D. Maize, Gang Qiu, Chien-Ting Wu, Ali Shakouri, Muhammad A. Alam & Peide D. Ye. (2018). Steep-slope hysteresis-free negative capacitance MoS2 transistor. Nature Nanotechnology 13, (24–28)

45. R. Vogel ; P. J. Walsh Appl. Phys. Lett. 14, 216 (1969)

46. Asif Islam Khan, Debanjan Bhowmik, Pu Yu,Sung Joo Kim, Xiaoqing Pan, Ramamoorthy Ramesh, Sayeef Salahuddin. Experimental evidence of ferroelectric negative capacitance in nanoscale heterostructures. Applied physics letters 99, 113501 (2011)

CHAPTER 2

LITERATURE SURVEY

2.1 Discovery of Negative Capacitance (NC):

The discovery of NC goes back to 1969 when it was observed for the first time in amorphous chalcogenide thin films by Vogel and Walsh [1]. During a program investigating the rapid electrical switching in disordered materials, low-signal ac capacitance measurements were made as a function of voltage and temperature on glassy chalcogenide thin films. The capacitance at zero bias voltage follows a Curie-Weiss law. However, above room temperature the capacitance of the films was found to decrease rapidly at bias voltages near threshold and displayed a negative value as biasing became close to the threshold of switching as well as at very low temperatures. It was observed that, at voltage below V_{th}, the film is in a high resistance state while above V_{th}, the films switch to a highly conducting state. A dielectric phase transition appears implicated in the switching process. The capacitance is substantially constant with voltage up to within about 5 V of threshold. Within about 5 V of threshold the measured capacitance starts to drop and goes to zero about 2 V below threshold and then effectively becomes negative. It has been observed that the measured capacitance becomes negative even at zero bias voltage when the temperature is lowered below -30°C. Since then it has been observed in a vast category of systems including electro-rheological fluid, thin films of inorganic, organic, compounds and composites.

Negative capacitance has been detected by the teams led by Prof. Sayeef Salahuddin and Prof. Ramesh [2]. The study detects negative capacitance in ferroelectrics. In the research led by Salahuddin *et. al.*, from University of Berkeley, a technique to measure the phenomenon has been proposed for the first time. The Boltzmann distribution of electrons poses a fundamental barrier to lowering energy dissipation in conventional electronics, often termed as Boltzmann Tyranny. Negative capacitance in ferroelectric materials, which stems from the stored energy of a phase transition, could provide a solution, but a direct measurement of negative capacitance has so far been elusive. But in the work done by Salahuddin and his group, the observation of negative capacitance in a thin, epitaxial ferroelectric film has been reported. When a voltage pulse is applied, the voltage across the ferroelectric capacitor is found to be decreasing with time in exactly the opposite direction to which voltage for a regular capacitor should change. Analysis of this 'inductance' - like behaviour from a capacitor presents an unprecedented insight into the intrinsic energy profile of the ferroelectric material and could pave the way for completely new applications. In

Salahuddin's work it has been shown that negative capacitance can be used to provide voltage amplification for low power nanoscale devices. Also, negative capacitance transistors have been made.

2.2 Theory and Application

In 1969, Vogel and Walsh reported the negative capacitance (NC) for the first time. Negative capacitance is generally known in semiconductors and ferroelectrics.

There have been two types of NC phenomena observed regarding mesoscopic and microscopic homo/heterojunctions – (i) transition type and (ii) Universal Debye response (UDR) type [3]. Transition type NC is more common in the literature characterized by gradual transition of capacitance from negative to positive regime or vice-versa and is dominated by Maxwell-Wagner interfacial relaxation. On the other hand, UDR type is characterized by negative static plane of NC associated with dipolar relaxation either at low or in the high frequency region.

A capacitor is a device that consists of two metallic electrodes separated by a dielectric material. When voltage is applied to electrodes, an electric field is created and the dielectric responds by polarizing. Positive charge will collect on one plate and negative charge on the other. Materials with the highest dielectric constants can be successfully used to achieve negative capacitance (NC) in a circuit.

A capacitor works by storing energy electrostatically in an electric field. The time it takes to discharge a capacitor is usually only a split second. And so is the time to recharge it. For negative capacitance, the capacitance (charge divided by voltage) has a negative value. For all positive capacitance dispersion, the magnitude of capacitance decreases sharply with the increasing frequency due to charge trapping but for NC the magnitude of the capacitance increases with the increase of frequency. This is important to note that with increasing external bias the NC dispersion extends to the larger frequency.

Physical mechanisms considered for NC observation are very clearly distinguishable for different devices, e.g., charge trapping, minority carrier injection, space charge effect,

interface states, contact injection, etc. These apparently divergent interpretations can be considered as

the manifestations of similar dipole dynamics such as nonlinearity and delocalization of carriers [3].

Physically, the relaxation of dipoles has definitive dependence on the charge localization function around them. Although most of the NC observation has been attributed to the presence of significant minority carrier concentration, dependence of the NC on charge localization has not been demonstrated even qualitatively.

Ferroelectric materials and some semiconductor materials have the ability to show negative capacitance.

Ferroelectricity is a characteristic of certain materials that have a spontaneous electric polarization that can be reversed by the application of an external electric field. All ferroelectrics are pyroelectric, with the additional property that their natural electrical polarization is reversible.
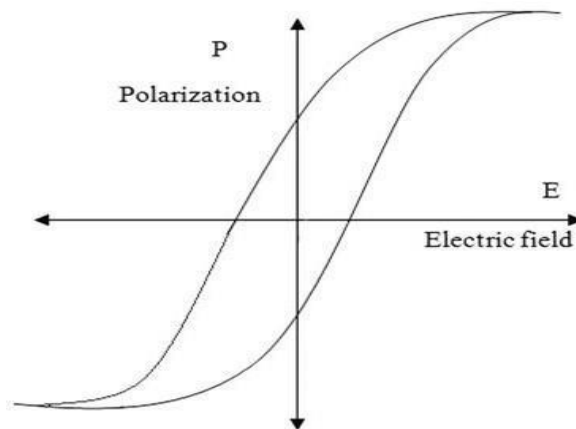
Fig 2.1 : Hysteresis loop in ferroelectric materials

2.2.1 Negative Capacitance in Ferroelectrics:

❖ Negative capacitance in ferroelectrics can be directly measured by putting a large resistance between the voltage supply and the electrodes of the ferroelectric capacitor.

❖ Ferroelectrics behave nonlinearly, meaning that small increments in voltage can lead to disproportionate changes in ferroelectric polarization. This is because ferroelectrics have a spontaneous polarization that flips above a certain critical voltage (known as coercive voltage), yielding an enormous and sudden accumulation of bound charge at the material's surface. Such 'ferroelectric charge' can momentarily exceed the free charge supplied to the electrodes by a power source, particularly if the latter is slowed down.

❖ By inserting a resistance between the voltage source and the ferroelectric, Salahuddin and colleagues have slowed down the charge supplied by the external voltage source long enough to allow for the measurement of a momentary decrease in voltage across the ferroelectric using a conventional oscilloscope. As the charge is still increasing while the voltage decreases, the resulting capacitance is negative.

❖ Of course, such a negative capacitance is a transient phenomenon, and when capacitance is integrated over a whole voltage cycle the negative component will always be smaller than the positive one.

2.2.2 Limitations in Ferroelectrics:

❖ The ferroelectric 'negative-capacitance state' is intrinsically unstable because it exists only around the tipping point between the two thermodynamically stable polarization states. This complicates practical implementation.

❖ The negative-capacitance state observed by Salahuddin and colleagues lives only for as long as the ferroelectric polarization is switching, and remains unscreened.

❖ To prevent screening & maintain a negative-capacitance state, an insulator could be inserted at the interface between the ferroelectric and the electrode. But in doing so, further problems arise: First, an unscreened ferroelectric is an unstable ferroelectric

that either tries to screen its polarization with any available charge carriers or make its own net polarization „disappear" by reducing its Curie temperature or creating equal fractions of domains with antiparallel polarization. Second, some of the voltage would be dropped across the dielectric layer, so a higher total external voltage would be required, which is contrary to the initial purpose of using negative capacitance.

❖ Also, there are switching-speed limitations of ferroelectric negative capacitance FETs.

2.2.3 Negative Capacitance in Semiconductors:

❖ The NC effect has been displayed by a variety of electronic devices, made of crystalline or amorphous semiconductors.

❖ Theoretical interpretations of NC phenomenon were often based on considerations of purely electrostatic charge redistribution inside the device.

❖ The real devices contain contacts, which can influence strongly the small-signal characteristics and result in NC. Indeed, it was verified that in many cases the NC phenomenon was caused by the contact or interface effects.

2.2.4 Applications of Negative Capacitance:

❖ Use of negative capacitance to provide voltage amplification for low power nanoscale devices.

❖ The negative capacitance of ferroelectrics is thought to offer a solution to a bottleneck in transistor miniaturization: transistors are becoming too small and clock-speed too fast to remove the heat generated during switching, resulting in increased power dissipation and overheating. Because the dissipated power is proportional to the square of the voltage, a potential solution is to reduce the voltage applied.

❖ The negative capacitance effect has the potential to lead to very low voltage yet high performance electronic switches.

- ❖ The experimental measurement of negative capacitance in ferroelectrics is a step forward in the battle for overcoming the „Boltzmann tyranny‟ that limits the performance of conventional transistors.

- ❖ Advantages for using it for designing new electronic devices & specifically ultra-efficient transistors.

- ❖ Negative capacitance phenomena observed in low quality CZT (Cadmium Zinc Telluride) radiation detectors at room temperature.

- ❖ Negative capacitance ferroelectric (FE) field-effect transistor (FeFET) is promising to address the issue of the increasing power density in digital circuit by realizing sub-60 mV/decade sub-threshold swing.

- ❖ Using the ferroelectric material in a transistor's gate allows for negative capacitance, which could result in far lower power consumption to operate a transistor.

- ❖ Negative capacitor-FET promises to lower supply voltage and power dissipation.

- ❖ Self-heating in transistors could be minimized with this NC effect.

- ❖ Feasibility of negative capacitance at room temperature is possible using a lead-free perovskite ferroelectric of varying thickness. The robust material can be integrated into CMOS or included as a performance booster within innovative devices such as tunnel field effect transistors in order to realize a future low power technology.

- ❖ NC measured experimentally has been sometimes (incorrectly) attributed to instrumental problems, such as parasitic inductance or poor measurement equipment calibration. Some told that the decrease of capacitance (minimum) is of relative nature and in fact is nothing but the interim capacitance drop at subsequent time t2 as compare to previous time t1. In this comparative sense it may be read as negative phenomenon. But it was a misconception that absolute negative value C = |c| simply doesn't exist (like negative mass or viscosity or temperature in Kelvin scale, etc.). So, some misinterpreted that negative capacitance as an entity which simply doesn't exist.

Also, negative capacitance has been interpreted as a dynamic effect when one measures electrical response in materials (non-linearity might be playing a role). Some researchers said that, it is apparently a result of response current being non-monotonic, going through a minimum (in time) and then increasing before becoming time independent. This happens even in perfect mono-crystals with residual deep defects and/or under dc bias voltage load. As an example, is shown a plot of complex capacitance, measured in a perfect mono-crystalline Silicon sample (Schottky-Schottky contacts) dc biased to -0.1 Volt.

The errors of Capacitance-Voltage (C-V) characteristic measurements for ultra-thin gate dielectrics in MOS capacitor were studied by I-V method. It was found that there are two reasons for the errors at low measurement frequencies: (1) the deviation of the phase angle of measured impedance, which causes apparent "Negative capacitance" that is inversely proportional to the measurement frequency. (2) AC-response in non-Ohmic conducting materials that form MOS capacitors, which may result in "Negative" or "Excess" capacitance. It was also found that the errors due to phase angle inaccuracy could be eliminated both by the phase rotation correction of the impedance and by measurements at higher frequencies.

The errors due to non-Ohmic conduction should be avoided by measurements of MOS-capacitors with small gate areas and low parasitic AC impedance.

The existence of a negative static dielectric constant has drawn a great deal of theoretical controversy. Experimentally, one has never been observed. However, low frequency negative capacitance has been widely reported in fields including physics, chemistry, biology, geology and electronics. This wide variety of systems possesses an extremely diverse set of physical processes that surprisingly share similar characteristics.

Materials and devices that exhibit negative capacitance (NC) are beginning to become quite common. It has been observed in samples as different as crystalline and amorphous semiconductor devices, organic compounds, composite materials/nanomaterials, electrochemical cells, geological samples, biological membranes, and even moist surfaces. Furthermore, it has been shown that NCs can originate at interfaces as well as in the bulk of the materials. However, they do typically share several common features: they arise in the presence of a dc bias; the I-V characteristic is superlinear, i.e., the in-phase conductance $1/R_{ac}$ increases with the dc bias; and they possess a strong dispersion, such as a plasmalike admittance $1/R_{ac}+i\omega C$ α, where ω and τ are the frequency and a time scale, respectively. In fact, NC has not been reported in linear systems below microwave frequencies with good

reason: the parameter τ should be interpreted as the carrier relaxation time $<< 10^{-9}$ s, and lead to a ωC term negligibly small against the in-phase $1/R_{ac}$. Previously, plasmalike NC has been reported in an electrorheological (ER) fluid. It can also be argued that such NC should represent a negative-differential dielectric constant (a property whose very existence has long been debated) ,if the associated nonlinearity and dispersion are bulk phenomena.

A negative capacitance (NC) effect, observed in a variety of semiconductor devices. The correct interpretation of NC can be based on the analysis of the time-domain transient current in response to a small voltage step or impulse, involving a self-consistent treatment of all relevant physical effects (carrier transport, injection, recharging etc.). The general relationships between the transient current in the time-domain and capacitance in the frequency domain follow from the properties of the Fourier transform are independent of the particular physical processes and applicable to all types of electronic devices.

Capacitance characteristics provide a powerful spectroscopic method for the non-destructive testing of semiconductor devices and evaluation of their structural and physical parameters. Capacitance or admittance spectroscopy also gives an insight into the device physics, provided that the experimental data are correctly interpreted. Quite often the capacitance exhibits highly non-trivial characteristics, most notable of which is the phenomenon of negative capacitance (NC).

The NC effect has been displayed by a variety of electronic devices, both heterostructures and homostructures, made of crystalline or amorphous semiconductors, such as Si, Ge, GaAs, HgCdTe, Se, and others [5]. These devices include p-n junctions, Schottky diodes, metal-insulator-metal devices, MESFETs, metal-insulator-semiconductor structures, weakly coupled superlattices, quantum mesoscopic devices, quantum well infrared photodetectors, and so on.

Microscopic physical mechanisms of NC in different devices are, obviously, different, but there should be some general principle behind NC common to all types of devices. But the concept of NC is still not widely recognized. Moreover, there is no adequate discussion of capacitance in classical texts on physics of semiconductor devices. The NC effect reported in the literature has been often referred to as "anomalous" or "abnormal" [5]. Regrettably, in many cases experimental NC data were not reported in the literature due to the confusion caused by the NC effect.

On the other hand, theoretical interpretations of the NC phenomenon were often based on considerations of purely electrostatic charge redistribution inside the device. However, a simple incremental charge method of capacitance calculation can be incorrect in the case of large conduction current (which often accompanies NC phenomenon), and more rigorous approaches considering transient response in the time or frequency domain should be used.

Recently, the NC effect in homogeneous (barrier-free) semiconductor structures has been considered theoretically. It was shown that NC can appear if the conductivity is inertial (i. e. current lags behind voltage) and the reactive component of the conduction current is larger than the displacement current. This situation can occur, for example, in structures with Drude conductivity, or in the case of impact ionization of impurity atoms.

NC appears in the case of the non-monotonic or positive-valued behavior of the time-derivative of the transient current in response to a small voltage step. The huge NC effect/phenomenon in quantum well infrared photodetectors (QWIPs) is due to the non-equilibrium transient injection from the emitter, caused by the injecting contact and the inertia of the QW recharging processes [5].

2.3 Contemporary Research

The concept of negative capacitance (NC) is a new and researchable topic. It is an innovative property that has been seen in many ferroelectric and some semiconductor materials and has raised obvious curiosity and varied questions among scientists about its origin and applications; though the proper reason behind the origin of NC is still a debatable topic and is under on-going research. Here, some contemporary interesting researches by various research institutes and scientists have been mentioned below:

2.3.1. Negative Capacitance in Ferroelectrics at Room Temperature

Effective negative capacitance has been observed at room temperature in engineered devices, where it is stabilized by the presence of a paraelectric material [6]. The concept of ferroelectrics displaying e ective negative permittivity has led to the speculation that its inclusion in the gate stack of a metal oxide semiconductor field e ect transistor (MOSFET) will reduce the subthreshold swing of complementary metal oxide semiconductor (CMOS) devices below 60 mV/dec. For a gate stack comprising a thin ferroelectric layer on top of a thin insulator layer, the channel potential (Ψ_s) can change more than the gate voltage (V_g) thus providing a step-up voltage transformer and S < 60 mV/dec. If this can be engineered, it heralds a transformation of future integrated circuits (ICs), reducing the o -state current (I_{off})

and/or supply voltage (V_{DD}) that otherwise limits Moore"s Law, as heat generated during switching cannot be removed. The idea has led to the search for unambiguous experimental evidence of negative capacitance in candidate ferroelectrics at room temperature as a step toward this ambition. Alternative solutions under investigation for low energy devices include the use of impact ionization (requiring high E fields so unlikely to be useful at small geometries) and tunneling currents (involving high series resistance which will slow devices).

Ferroelectric materials display spontaneous electric polarization, below a critical temperature Tc, which can be aligned by an applied electric field. A permanent dipole moment remains when the electric field is removed. An unstable region of negative dP/dE accompanies P−E hysteresis corresponding with negative capacitance, but it is energetically unstable inisolation. It arises from an increasing alignment of electric dipoles as the applied electric field increases, which increases the polarization; when the field is removed there is a nonzero remnant polarization
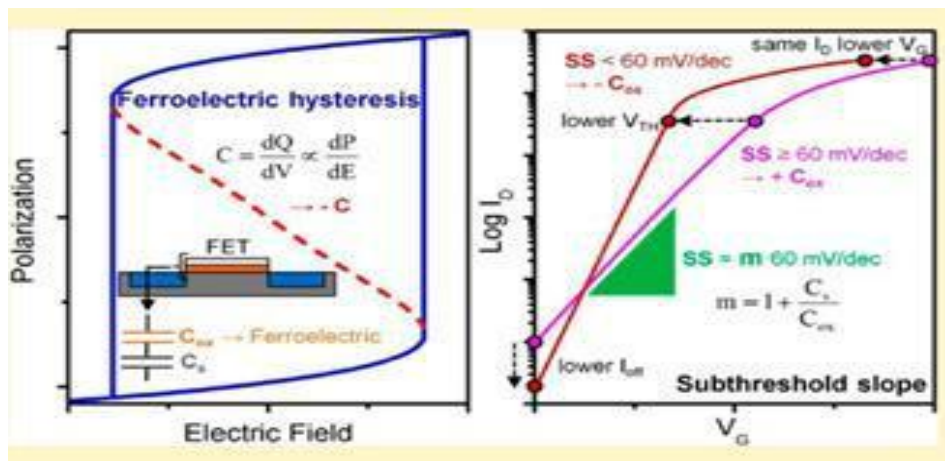
Fig 2.2 : Hysteresis in plots of polarization versus applied electric field [6]

Experimental evidence for negative capacitance has proved elusive, although proposals to stabilize it, in series with positive capacitance, have been put forward. Here, experimental demonstration of effective negative capacitance in devices consisting of the ferroelectric $BaTiO_3$ in series with the paraelectric $SrTiO_3$ at room temperature has been demonstrated. The low Curie temperature of $BaTiO_3$ allows room temperature stabilization of negative capacitance in a perovskite for the first time. It is repeatable and demonstrated at high frequencies. Attempts have been made to observe experimentally the characteristics of negative capacitance in ferroelectrics. However, this has proven elusive for ferroelectrics in

isolation, because it corresponds with a negative energy density and so is unstable. In order to observe negative capacitance, it must be incorporated into a device with overall positive capacitance (and therefore positive energy density). Specifically, negative capacitance can be stabilized by using a bilayer metal-insulator-metal (MIM) parallel plate capacitor, as shown in Figure a. The total capacitance C_t is the sum of the inverse capacitances of each layer where, C_1 is the capacitance from a paraelectric material and C_2 is the capacitance of a ferroelectric material.
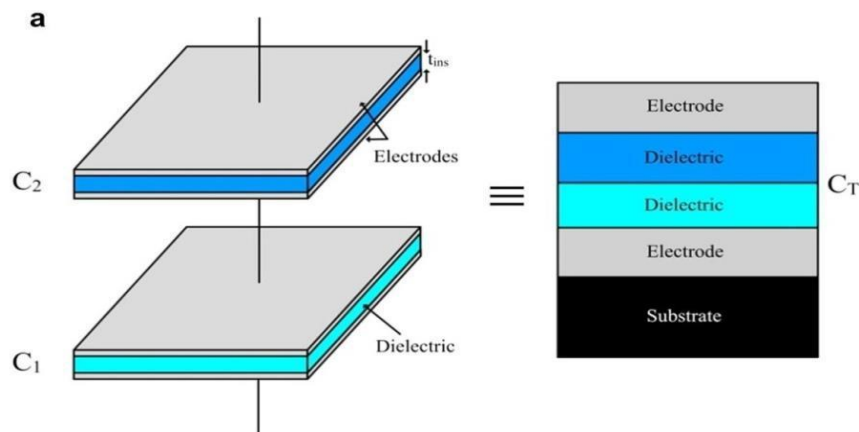
Fig 2.3 a: The series capacitance is modelled using a metal-insulator-metal stack on a substrate. Figure 2.4 a and Figure 2.4 b show series capacitance configuration and plot of 2 capacitors. Figure 2.3 b shows the theoretical relationship between C_t, C_1, and C_2 based on eq. (1) [6]

It is observed that as C_2 varies from positive to negative, C_t undergoes different changes to its overall stability. Region b is identified as the design window where e ective negative capacitance is stabilized, corresponding with a positive total energy density. Moreover, the total capacitance C_t is larger than the constituent positive capacitance C_1 due to the negative capacitance C_2. Region a is unstable, as it has a total energy density that is negative, while region c comprises two positive capacitances in series that combine to have a reduced total capacitance.
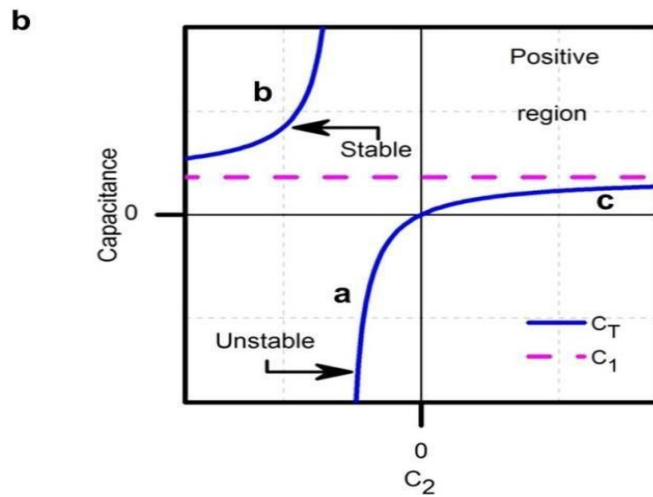
Fig 2.4 b : The solid line (blue) represents the total capacitance of the system with the dashed line showing the positive capacitor in the series. Data is given as a function of the remaining capacitor contribution C_2, which is allowed to become negative. Standard analysis for the total capacitance is representative of the right half of the figure [6]

The capacitance is always positive for a ferroelectric under the critical temperature, and polarization switching occurs when the field is reversed. The negative capacitance region due to the negative energy curvature is unstable in isolation. Hence, negative capacitance is never measured for single layer ferroelectrics and should be stabilized in a series capacitance system.

Effective negative capacitance may only be inferred from experiment using specific bilayer MIM device designs and conditions, as described above. A bilayer C_t of $SrTiO_3$ is paraelectric and has a capacitance C_1 and $BaTiO_3$ is ferroelectric below the Curie temperature, T_C, and has a capacitance C_2. At a low temperature of 100 K, the total capacitance displays ferroelectric properties. As a result, the negative capacitance will be energetically unstable and not observable. This corresponds to operations in region a, as shown in Figure 2.4 b. At room temperature, this bilayer design shows an overall positive capacitance as seen by the single minimum in C_t at P = 0 and so negative capacitance could be observed. This is the ideal stable operation window, as described in region b in Figure b. At a temperature of 500 K , above T_C the $BaTiO_3$ layer has become paraelectric and so the overall capacitance comes from two paraelectric contributions. In this case, it follows that the total capacitance C_T is less than C_1 or C_2, corresponding to region c in Figure 2.4 b. In this study, experimental evidence is presented to demonstrate e ective negative capacitance at room temperature is possible in a thin film of the ferroelectric $BaTiO_3$. Any hysteresis behavior is absent from the capacitance measurements in these bilayer devices, which show

tunable paraelectric capacitance properties. The tunable capacitance trends are also shown to increase as the thickness of BaTiO3 increases. This is consistent with the insulator becoming dominated with BaTiO3 due to its higher Curie temperature T_c.

The results indicate the likelihood of negative capacitance as a technology for reducing the sub-threshold swing. The study highlighted that using low Curie temperature materials will enable negative capacitance stabilization at room temperature, such as BaTiO3 used here.

2.3.2 Negative capacitance in light-emitting devices

The forward electrical characteristics in LEDs and LDs are important for analyzing their performance, microscopic mechanisms and practical applications, where the diodes are under dynamic regimes [7]. In the forward admittance measurements, negative capacitance (NC) behavior has been observed in Schottky diodes, p–n junctions, quantum well infrared photodetectors (QWIPs) and homojunction far-infrared detectors. But in these reports only the measured apparent capacitance values of the devices were given without calculating forward junction capacitance. In fact, the junction capacitance may be much larger than the measured apparent capacitance at high forward biases. And the calculation of junction capacitance is necessary in order to get the quantitative interpretation of the NC effect invarious diodes convincingly. Remarkable NC phenomenon was observed in LEDs and LDs in the ac admittance measurement. Further experiments showed that remarkable NC was always accompanied by light emission and confirmed as the capacitance behaviour of the diode but not other effect. And the mechanism of NC in LEDs and LDs is very different from that in other devices. It shows that the negative capacitance behavior in light-emitting diodes has great relation to injected carriers recombination in the active region of luminescence.

2.3.3 Negative capacitance in amorphous semiconductor chalcogenide thin films

Certain amorphous materials exhibit rapid electrical switching [1]. During a program investigating the rapid electrical switching in disordered materials, low-signal ac capacitance measurements were made as a function of voltage and temperature on glassy chalcogenide thin films. The capacitance at zero bias voltage follows a Curie-Weiss law. However, above room temperature the capacitance of the films was found to decrease rapidly at bias voltages near threshold and displayed a negative value as biasing became close to the threshold of switching as well as at very low temperatures. The capacitance measured is essentially an incremental ac equivalent parallel capacitance of the film and contacts. Various dc bias voltages were applied across the sample. The frequency used was generally 100 kHz. The films are commercially made by flash evaporation from pre-melted solid ingots of approximate weight composition: 49% Te, 33% As, 6% Ge, 3% Si, and 9% Ga. The variation in their capacitance was evaluated as a function of temperature and electric field in the high-resistance state. Thus, it has been observed that at low temperatures, and at fields near the threshold of switching for higher temperatures, the open-circuit incremental ac capacitance becomes negative.

2.3.4. Negative Capacitance Transistors

A ferroelectric material stores energy from phase transition and in doing so it tends itself to be biased at a state where its capacitance is negative. When such a negative capacitance is added in series to the gate of a, sub-threshold swing in a Field Effect Transistor (FET), it is possible to reduce the sub-threshold swing below 60 mV/decade, without changing the transport physics of the FET. Not having to change the transport physics means that the ON current can be high while the supply voltage can be reduced significantly. Therefore, the negative capacitance effect has the potential to lead to very low voltage yet high performance electronic switches.
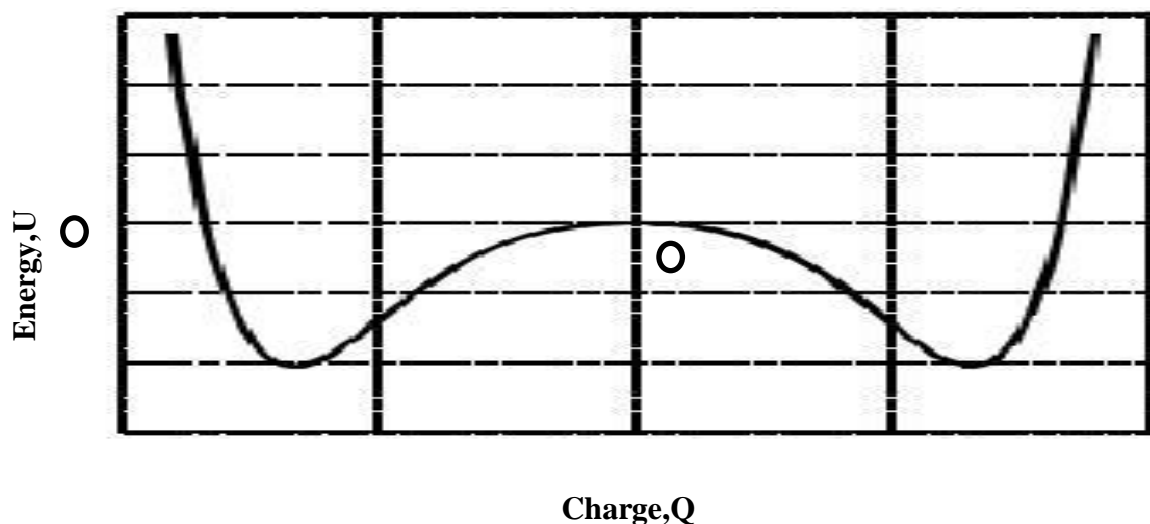
Fig 2.5 : Energy Landscape of a FE Material [8]

Another way to increase the sharpness of the FET turn-on is to incorporate an internal gain mechanism so that a small voltage swing on the gate electrode causes a larger swing of the internal potential that gates the flow of current. Salahuddin and Datta proposed a device with a gate insulator stack consisting of a layer of ferroelectric material sandwiched between conventional dielectric layers. The energy barrier presented by this gate structure to charge injection depends on the polarization of the ferroelectric layer, which, because it arises from a collective effect, switches abruptly between two polarization states. A key insight was the recognition that layer thicknesses and material properties could be engineered so as to greatly suppress the undesirable hysteretic behavior that would normally be expected from such a gate structure while still amplifying the effect of the gate potential on the channel potential. One potential drawback is that the shortest reported ferroelectric switching times, 70 to 90 ps, are too long to be of interest for fast FET logic, where switching can occur in 1 ps or less. But Kopp and Mannhart have predicted similar effects in electronic systems exhibiting strong electron exchange and correlation effects.

2.3.5 Negative capacitance of GaAs homojunction far-infrared detectors

High performance far-infrared ~FIR ~40 ± 200 mm semi-conductor detectors as well as large focal plane arrays are required for space astronomy applications, such as the National Aeronautics and Space Administration's (NASA) airborne mission, Stratospheric Observatory for Infrared Astronomy (SOFIA), and the ESA's Far-infrared and Sub-mm Telescope (FIRST) programs [9]. Si or GaAs homojunction interfacial work-function internal photoemission (HIWIP) far-infrared detectors can compete with extrinsic Ge photocon-ductors unstressed or stressed and Ge block-impurity-band (BIB) detectors due to the material advantage of Si or GaAs over Ge. The detection mechanism of HIWIP

detectors involves infrared absorption in the highly doped emitter layers mainly by free carrier absorption followed by the internal photoemission of photoexcited carriers across the junction barrier and then collection. The detector cut-off wavelength is determined by the interfacial barrier height between the emitter layers and undoped intrinsic layers. Significant progress has already been achieved in the development of *p*-GaAs HIWIP FIR detectors, resulting in a responsivity of 3.1 A/W, detectivity of 5.9310 cmAHz/W, with cut-off wavelengths as long as 100 *m*m. The present GaAs HIWIP FIR detector displays symmetric *C-V* characteristics under positive and negative biases, unlike the asymmetric behaviour in GaAs/AlGaAs quantum well infrared photodetectors ~QWIPs due to dopant migration in the growth direction. The symmetric behavior can also be observed in its dark current-voltage and noise-voltage measurements. However, similar to the case of QWIPs, the capacitance displays a maximum at zero bias, decreases rapidly with increasing bias voltage, and reaches negative values at higher biases. The decrease is more rapid at low frequencies. The capacitance at zero bias decreases with frequency, approaching the value of the geometrical capacitance, C_0, at high frequencies.

Negative capacitance phenomenon has been displayed by a variety of electronic devices, such as p-n junctions, metal-semiconductor Schottky diodes, and GaAs/AlGaAs QWIPs. The microscopic physical mechanisms of the negative capacitance in different devices have been ascribed mainly to the contact injection, interface state, or minority-carrier injection effects. The negative capacitance phenomenon could be interpreted by transient current analysis and was attributed to be a consequence of the kinetic reactivity due to the inertia - delay of the change in the current owing in the structure as a result of changing the applied voltage. The negative capacitance caused by the injection of minority carriers can be observed only at forward biases and low frequencies. The HIWIP structures show negative capacitance even at high frequencies and negative bias.

In summary, a negative capacitance behavior in p-GaAs HIWIP far-infrared detectors has been observed. The phenomenon can be attributed to the carrier capture and emission from the interface states. The negative capacitance indicates the existence of occupied states at the interfaces between emitter layers and intrinsic layers, which is in agreement with the detector dark current, response and noise measurements. Unlike in other devices, even up to 1 MHz in HIWIP, the negative capacitance value keeps increasing with frequency, giving a stronger effect.

2.3.6 Negative capacitance in organic semiconductor devices

Negative capacitance has been reported at low frequencies in organic semiconductor based diodes and show that it appears only under bipolar injection conditions [10]. They account quantitatively for this phenomenon by the recombination current due to electron-hole annihilation. Simple addition of the recombination current to the well-established model of space charge limited current in the presence of traps yields excellent points to the experimentally measured admittance data. The dependence of the extracted characteristic recombination time on the bias voltage is indicative of a charge recombination process which is mediated by localized traps. In admittance spectroscopy of organic semiconductor devices, negative capacitance values arise at low frequency and high voltages. Here, it has been shown that negative capacitance originates from self-heating induced current enhancement.

2.3.7 Plasmalike negative capacitance in nano-colloids

A nano-colloid represents a dispersed phase and is composed of nanoparticles [11]. A negative capacitance has been observed in a nano-colloid between 0.1 and 10^{-5} Hz. The response is linear over a broad range of conditions. The low-υ dispersions of both the resistance and capacitance are consistent with the free-carrier plasma model, while the transient behavior demonstrates a possible energy storage mechanism. A negative capacitance in an ER fluid. Linearity is observed over broad ranges of V_{dc} and V_{ac}. The dispersions in both C and R channels and the associated energy storage/conversion demonstrate that plasmalike excitations are present. This demonstrates that impedances can be drastically changed through mesostructures and open the door for novel nanomaterials.

2.4 References :

1. R. Vogel ; P. J. Walsh. Negative capacitance in amorphous semiconductor chalcogenide thin films. Appl. Phys. Lett. 14, 216 (1969)

2. Khan. A.I , Chatterjee. K, Wang. B, Drapcho. S, You. L, Serrao. C, Bakaul. S.R, Ramesh.and R , Salahuddin. S. Negative capacitance in a ferroelectric capacitor. Nature Materials volume 14, pages 182–186 (2015)

3. Mazumder. N, Sen. D, Ghorai. U.K , Roy. R, Saha. S, Das N.S , Chattopadhyay. K.K , J. Phys. Chem. Lett. 4, 3539 (2013).

4. .Salahuddin.S ; Datta.S. Use of Negative Capacitance to Provide Voltage Amplification for Low Power Nanoscale Devices. Nano Lett., 2008, 8 (2), pp 405–410

5. https://www.researchgate.net/NegativeCapacitance01.doc.

6. M. Ershov, H. C. Liu, L. Li, M. Buchanan, Z. R. Wasilewski, and A. K. Jonscher. Negative capacitance e ect in semiconductor devices. Ieee transactions on electron devices.

7. Daniel J. R. Appleby, Nikhil K. Ponon, Kelvin S. K. Kwa, Bin Zou, Peter K. Petrov, Tianle Wang, and Neil M. Alford and Anthony O‟Neill. Experimental Observation of Negative Capacitance in Ferroelectrics at Room Temperature. Nano Letters.

8. C.Y. Zhu, L.F. Feng, C.D. Wang, H.X. Cong, G.Y. Zhang, Z.J. Yang, and Z.Z. Chen. Negative capacitance in light-emitting devices. Solid-State Electronics 53 (2009) 324–328.

9. Salahuddin. S. Review of Negative Capacitance Transistors.

10. A. G. U. Perera, W. Z. Shen, M. Ershov, H. C. Liu, and M. Buchanan et al. Negative capacitance of GaAs homojunction far-infrared detectors. : Appl. Phys. Lett. 74, 3167 (1999); doi: 10.1063/1.12416

11. E. Ehrenfreund, C. Lungenschmied, G. Dennler, H. Neugebauer, and N. S. Sariciftci. Negative capacitance in organic semiconductor devices: Bipolar injection and charge recombination mechanism. Applied physics letters 91, 012112 2007.

12. J. Shulman, S. Tsui, F. Chen, Y. Y. Xue, and C. W. Chu. Plasmalike negative capacitance in nanocolloids. Applied Physics Letters 90, 032902 (2007).

13. S. Salahuddin and S. Datta, Nano Lett. 8, 405 (2008).

14. C. D. Wang, C. Y. Zhu, G. Y. Zhang, J. Shen, and L. Li, IEEE Trans. Electron Devices 50, 1145 (2003).

15. C. Y. Zhu, L. F. Feng, C. D. Wang, H. X. Cong, G. Y. Zhang, Z. J. Yang, and Z. Z. Chen, Solid-State Electron. 53, 324 (2009).

16. J. Shulman, Y. Y. Xue, S. Tsui, F. Chen, C. W. Chu. General mechanism for negative capacitance phenomena. Physical review B 80, 134202 2009.

17. Physics of Ferroelectrics: A Modern Perspective, Topics in Applied Physics, edited by K. Rabe, C. H. Ahn, and J.-M. Triscone (Springer, Berlin, 2007), Vol. 105.

18. Salahuddin, S.; Datta, S. Can the subthreshold swing in a classical FET be lowered below 60mV/decade? IEEE Int. Electron Devices Meet. 2008.

19. Krowne, C. M.; Kirchoefer, S. W.; Chang, W.; Pond, J. M.; Alldredge, L. M. B. Examination of the Possibility of Negative Capacitance Using Ferroelectric Materials in Solid State Electronic Devices. Nano Lett. 2011, 11, 988−992.

20. Zhirnov, V. V. & Cavin, R. K. Negative Capacitance to the rescue? Nat. Nanotechnol. 2008, 3.

21. Knapp.E ; Ruhstaller.B. Analysis of negative capacitance and self-heating in organic semiconductor devices. Journal of Applied Physics 117, 135501 (2015)

22. Khan, A. I.; et al. Experimental evidence of ferroelectric negative capacitance in nanoscale heterostructures. Appl. Phys. Lett. 2011, 99, 113501.

23. M. Ershov, H. C. Liu, L. Li, M. Buchanan, Z. R. Wasilewski et al. Unusual capacitance behavior of quantum well infrared photodetectors. Appl. Phys. Lett. 70, 1828 (1997).

CHAPTER 3:
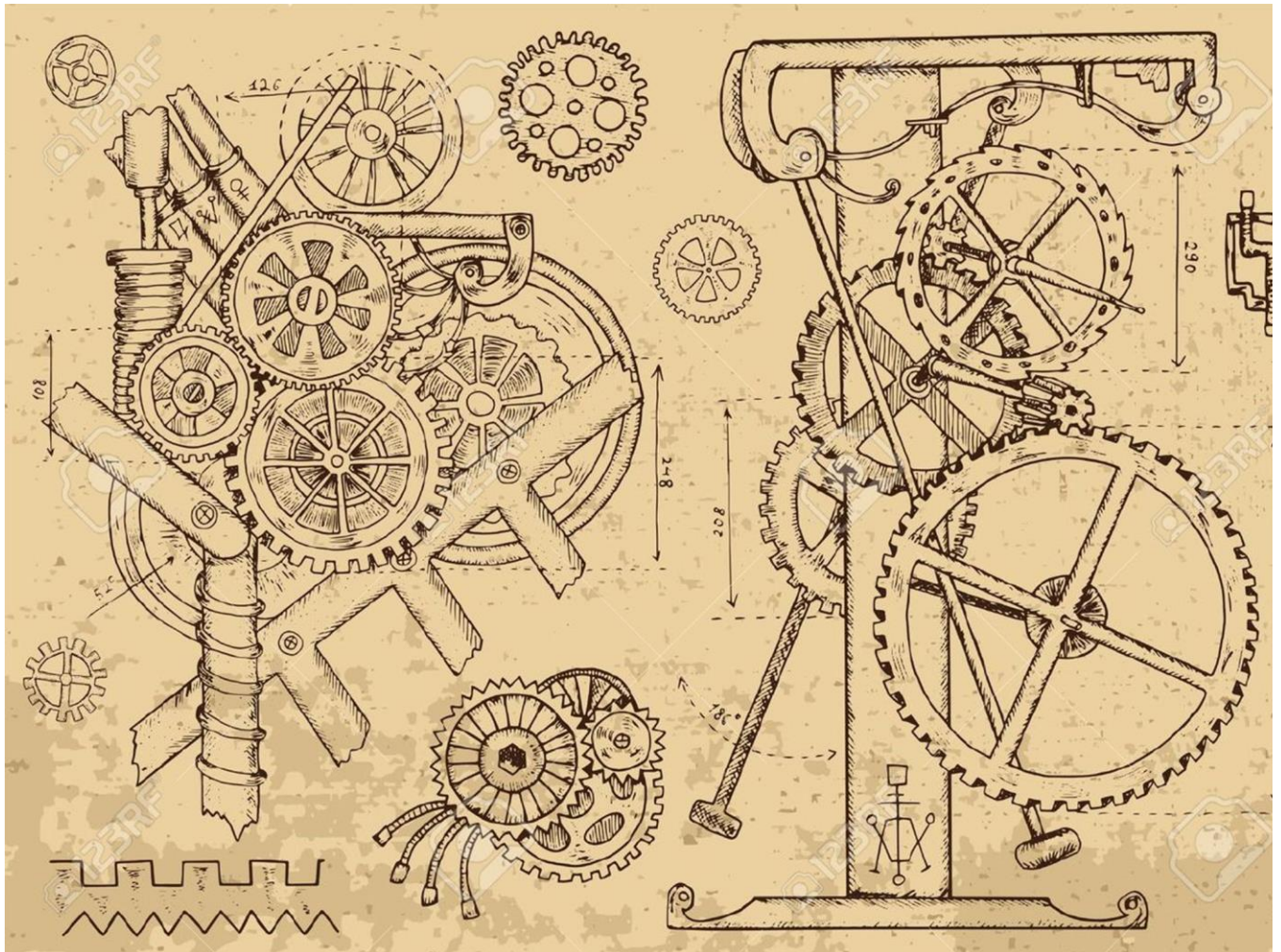
INSTRUMENTS

&

APPARATUS

3.1 Experimental set up:

3.1.1 Oven

Ovens are commonly used for solid state heating. Starting materials are heated and dried using oven at temperature $60 - 200$ ^{0}C for $15 - 20$ h. The temperature controller usually controls the rate of heating and maintains the temperature with an accuracy of ± 0.5 ^{0}C. **Fig.3.1** (a) shows the digital image of the oven used. A low temperature oven was used for drying the samples and also for certain hydrothermal reactions. The digital image of a typical oven is shown in **Fig.3.1**

Fig.3.1: Digital images Oven

3.1.2 Pelletizer

To prepare the pellets we have used a binder because in absence of binder the pellets were found to be very brittle. We have used polyvinyl alcohol (PVA) as the binding agent. To prepare the paste, suitable amount of PVA is mixed with deionized water and is mildly heated with constant stirring until an adhesive gel is formed. One or two drops of this paste are mixed with the oxide powder by a mortar and pestle. Then the powder is pressed into thick films of 12 mm diameter and about 1.5 – 2 mm of thickness under the uniaxial pressure of 1 GPa for 3 min using the pelletizer. The pellets are then sintered at 400 ℃ for 3 h to expel the PVA from the sample. Pellets are then connected with electrical contacts to perform characterizations.

Fig.3.2: Digital image of a Pelletizer

3.1.3. Magnetic Stirrer

The magnetic stirrer can stir the magnetic bit within the solution of the beaker through a revolving magnetic arrangement attached with it. A heater arrangement associated with the stirrer can heat the solution at a desired temperature and the temperature is controlled by a knob as shown in **Fig.3.3**.

Fig.3.3: Digital image of a magnetic stirrer

3.2 Characterization tools:

3.2.1 X–Ray diffractometer (XRD):

In 1895, x-ray is discovered by Röentgen. From the year 1912, the application of x– ray has started when the wave nature of x–ray was recognized from the x–ray diffraction by any crystals. X–ray diffraction by the different set of planes has been applied to identify crystal structures. The structural characterization of synthesized samples is carried out by recording the X–Ray Diffraction pattern of the samples. XRD pattern was taken using Cu K_α radiation (λ = 1.5406°A) (Rigaku–Ultima–III). The photograph is shown in the figure 3.3 below. The basic law involved in the crystal structure analysis is the Brag's law of diffraction. When monochromatic X–rays incident upon the atoms in a crystal lattice, each atom acts as a source of scattering. The crystal lattice acts as series of parallel reflecting planes and the reflected beams at certain angles form constructive interference which is an integral multiple of λ. This condition called Bragg's law is given by the relation,

$$2\text{dsin}\theta = n\lambda \qquad (3.1).$$

Where n is the order of diffraction and d is the spacing between two consecutive planes *and* λ is the wavelength of the x–rays, and Θ is the glancing angle. XRD studies of any sample give a whole range of information about the crystal structure, average crystallite size and various stresses in the thin film. Generally, the obtained experimental data of the sample are compared with the standard inorganic crystal structure database (ICSD) to confirm the phase purity of our synthesized samples.

From the shift in peak position, one can calculate the change of d–spacing, which signify the change of lattice constant under inhomogeneous or homogeneous strain. Inhomogeneous strain differs from crystallite to crystallite or within a single crystallite.

This causes the peak broadening which increases with $sin\ \theta$. This broadening also occurs from the crystalline size effect, but here the broadening is independent of $sin\ \theta$. If there is no inhomogeneous strain, the crystallite size, D can be calculated from the Scherrer's formula:

$$D = \frac{k\lambda}{\beta cos\theta} \qquad (3.2)$$

Where, β is the full width of height maximum (FWHM) of a diffraction peak, k is the Scherrer constant and θ is the diffraction angle [1–3].

Fig. 3.4 the X-ray diffractometer – Rigaku Ultima III.

3.2.2 X–ray photoelectron spectrometer (XPS)

Chemical Composition of the synthesized nanostructure, charge state of dopants, and purity of sample were analyzed by X–ray photoelectron spectroscopy (XPS, Specs, Germany). In photoelectron spectroscopy, photons are used to eject electrons from the bulk materials. Usually monochromatic, low energy X–rays are used to irradiate the sample which results in photoelectron emission from the atoms of the sample's surface and the kinetic energy distribution of the ejected photoelectrons is directly measured with the help of an electron spectrometer. As each surface atom possesses core–level electrons, the binding energy of each core–level electron is the characteristic of the atom and its specific orbit [1].

Since the energy of the incident X–rays is known, the measured kinetic energy of a core–level photoelectron peak can be directly assign to its characteristic binding energy. Therefore, XPS provides a means of elemental identification and the use of a standard set of sensitivity factors also provides a surface atomic composition. The kinetic energy (E_k) of these electrons is measured and their binding energy (E_b) can be calculated.
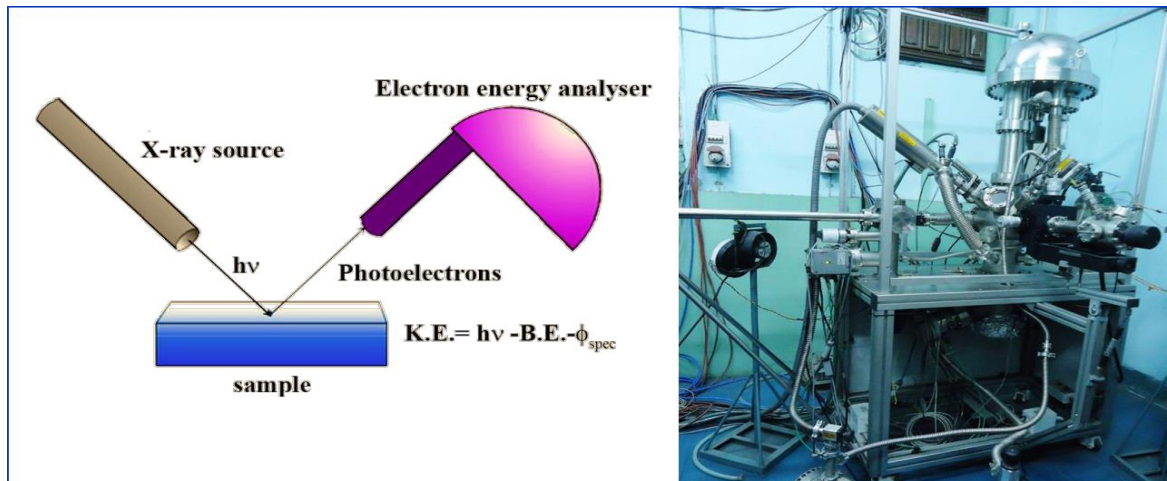
Fig. 3.5 Left: Schematic of the photo-excited electron emission in XPS instrument.Right: SPECS, HAS3500 XPS instrument

The determination of the electron binding energy is the goal of the spectrometer which is found using the following relation:

$$E_b = h\nu - E_k \qquad (3.3)$$

Where, *hv* is the X-ray energy (known) and E_k is the kinetic energy of the photoelectrons (measured) [4]. The mechanism of electron emission is shown schematically in figure 3.6
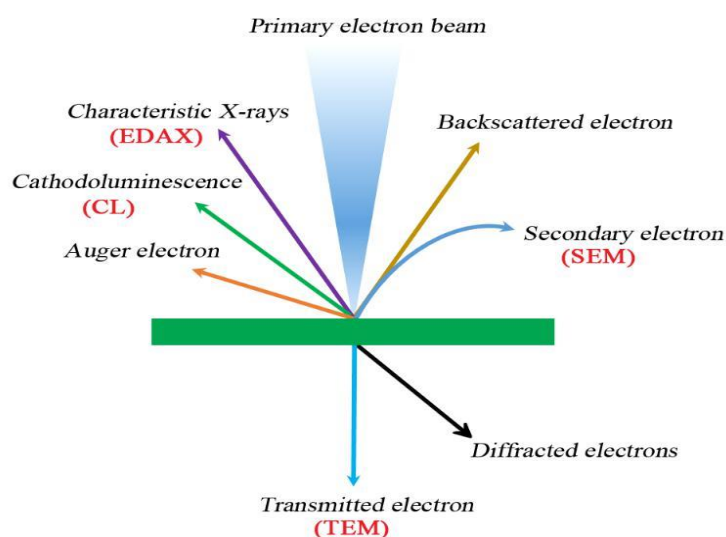
Fig. 3.6 Effects of electron bombardment on the material

Since binding energy of a photoelectron is profound to chemical surroundings of the atom, the chemical shifts in the binding energies of the photoelectron peaks arise due to the variations in electrostatic screening experienced by core level electrons. Various oxidation state, coordination number and molecular environment provide different chemical shifts that can be measured in a high-resolution (HR) XPS spectrum. In the present work, the chemical state of the constituent elements is examined by X–ray photoelectron spectroscopy using monochromatic Al K_α (hν = 1486.6 eV) X–ray source and a hemispherical analyzer (SPECS, HSA 3500). The photograph is shown in figure 3.4 (b).

Surface morphology

When an electron beam interacts with the atoms in a sample, individual incident electron undergoes two types of scattering: elastic and inelastic. In case of elastic scattering, only the trajectory changes, the kinetic energy and velocity remain constant. But in case of inelastic scattering, some incident electrons actually collide with and displace electrons from their orbits around nuclei of atoms of the sample. This interaction places the atom in an excited state.   This resulting electron vacancy is filled by an electron from a higher shell, and an X–ray photon   is emitted to balance the energy difference between the two electrons. The EDS X–ray detector (also called EDS or EDX) measures the number of emitted x-ray photons versus their energy. The energy of the x–ray is characteristic of the element from which the x–ray is emitted. Cathodoluminescence (CL) is the emission of photons of characteristic wavelengths from a material that is under high–energy electron bombardment. X–Rays, Cathodoluminescence and Auger electrons are the ways atoms relax by giving off its energy. Auger electrons are characteristic of the fine structure of the atom having energies between 280 eV (carbon) and   2.1 keV (sulfur). By discriminating between Auger electrons of various energies, a chemical analysis of the specimen surface can be made. Auger electrons are exploited in Auger Electron Spectroscopy tools (AES). This relaxation energy is the fingerprint of each element.Surface morphology is an important factor for nanostructured materials. The characterization tools used to analyze the morphology are described below [1].

### 3.2.3 Field emission scanning electron microscope (FESEM):

In standard electron microscopes, electrons are mostly generated by heating a tungsten filament (electron gun). They are also produced from a crystal of LaB_6. The use of LaB_6 results in a higher electron density in the beam and a better resolution than that with the conventional used device. In a field emission (FE) electron microscope, no heating but a so–called "cold" source is used. Field emission microscope is a type of electron microscope that is usually employed to investigate the surface of a sample by scanning it with a high energy beam of electrons. Here, the wave properties of electrons ($\lambda = h/p$, λ associated with a beam of electrons of momentum p) are used to obtain resolution. If the electrons are accelerated through a potential difference V, they acquire energy,

$$eV = \frac{p^2}{2m} => \lambda = \frac{h}{p} = \frac{h}{\sqrt{2meV}} \qquad (3.4)$$

So V = 100,000 V leads to $\lambda = 3.9 \times 10^{-12}$ m, which is about a hundredth of the separation of the atoms in molecules (~0.25 nm) or crystals [1].

In FESEM, the electron beam passes through objective lens deflect horizontally and vertically so that the beam scans the surface of the sample [Figure 3.7 (right)]. As the electrons penetrate the surface of the sample, a number of interactions occur that can result in the emission of electrons or photons from or through the surface. The generated secondary electrons are collected by the detector and converted into voltage. The amplified voltage is applied to the grid of the CRT which changes the intensity of the spot light. In this way an image is produced on the CRT; every point that the beam strikes on the sample is mapped directly onto a corresponding point on the screen [1, 6–7]. The schematic diagram of FESEM is presented in figure 3.7 (right). When an electron beam interacts with the atoms of a nano structures sample, each incident electron undergoes two types of scattering elastic and inelastic. In elastic scattering, only the trajectory changes and the kinetic energy and velocity

remain constant. In the case of inelastic scattering, the incident electrons displace electrons from the sample orbits around nuclei of atoms [1]. The electron interacts with the sample produces signal about the sample's morphology, composition and other properties. The morphologies of the synthesized nanomaterials are characterized with the help of field emission scanning electron microscopy (FESEM, S–4800). The photograph of the instrument is shown in figure 3.7 (left).
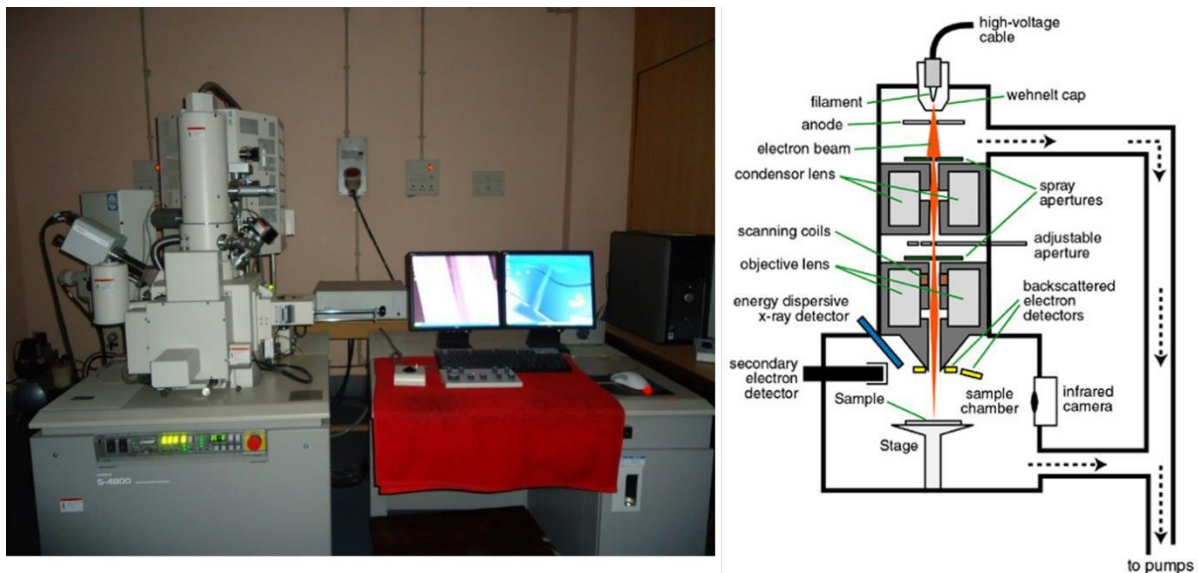
Figure 3.7   Left: Hitachi S4800 FESEM with EDX attachment, **Right: Simple schematic of FESEM instrument**

Energy Dispersive X–Ray (EDX) is one of the most versatile tools for analyzing the compositions of the synthesized samples. It is sometimes referred to also EDS or EDAX analysis. EDX is the integrated feature of both SEM and TEM. During EDX analysis, the specimen is bombarded with an electron beam inside electron microscope. The bombarding electrons collide with the specimen atom and knock some of them off in the process. The electrons vacated from the inner shell are eventually filled with the higher energy outer shell electrons and emit X–ray in this method. In this run, X–rays emitted from atoms represent the characteristics of the elements, and their intensity distribution represents the thickness–projected atom densities in the specimen. EDAX is a very important tool for identifying the chemical composition of a specimen [1, 6].

3.3 Theoretical support:

The description of the physical properties of interacting many-particle systems has been one of the most important goals of physics during this century. The problem is to derive the properties of many-particle systems from the quantum mechanical laws of nature. This requires the solution of a partial differential equation (the Schrödinger or Dirac equation) of 3N spatial variables and N spin variables (for electrons) where N is the number of particles in the system. During the past decade, computer simulations based on a quantum-mechanical description of the interactions between electrons and atomic nuclei have had an increasingly important impact on materials science, [10] not only in fundamental understanding but also with a strong emphasis toward materials design for future technologies. The simulations are performed with atomistic detail by solving the Schrödinger equation to obtain energies and forces, and require only the atomic numbers of the constituents as input, and should describe the bonding between the atoms with high accuracy. The Schrödinger equation for the complex many-atom, many-electron system is not analytically solvable, and numerical approaches have become invaluable for physics, chemistry and material science.

Recent advances in computer calculation techniques and hardware technology have accelerated theoretical approaches to developing new materials. [11] Trial-and-error approaches are still needed to finely adjust the functions of developed materials to practical applications, but in some cases, the basic direction for materials development can be obtained from theoretical and computational considerations. A breakthrough in these computational efforts was realized in 1964 when Walter Kohn and coworkers developed the density functional theory (DFT), a theory based on electron density, which is a function of only three spatial coordinates. [12] The Kohn–Sham equations of DFT cast the intractable complexity of the electron–electron interactions into an effective single-particle potential determined by the exchange-correlation functional. This functional (i.e., a function whose argument is

another function) describes the complex kinetic and energetic interactions of an electron with other electrons. In the following part, the two core elements of DFT, which are Hohenberg-Kohn theorem and the Kohn-Sham equations, are presented.

3.3.1 Elements of DFT

The behaviour of electrons in a crystal solid is governed by themany-body Schrodinger equation:

$$H(\Psi)=E(\Psi) \qquad (3.5)$$

It is generally appropriate to consider the electrons as either core or valence electrons. The core electrons are localized around the nuclei, and so the system can be treated as a number of valence electrons interacting with ion cores (nuclei and core electrons). Due to their significantly lower mass, the valence electrons can be assumed to react almost instantaneously to the motion of the ions - the ions appear stationary to the electrons, whereas the ions only respond to the time-averaged behavior of the electrons. This is the Born-Oppenheimer (or adiabatic) approximation, allowing the motion of the ions to be decoupled from that of the electrons. A stationary electronic state is then described by a wave function satisfying the many-electron time-independent Schrödinger equation:

$$\hat{H}\Psi=[\ \hat{T}+\hat{U}+\hat{V}\ ]\ \Psi=\sum_i^N \frac{-\hbar^2}{2m}\nabla_i^2 +\sum_i^N V(\overline{r_l})+\sum_{i<j}^N U\ (\overline{r_l},\overline{r_J})]\Psi = E\Psi \qquad (3.6)$$

where, for the N-electron system, Ĥ is the Hamiltonian, E is the total energy, T is the kinetic energy, V is the potential energy from the external field due to positively charged nuclei, and Û is the electron-electron interaction energy. The operators T and Û are called universal operators as they are the same for any N-electron system, while V is system dependent. This complicated many-particle equation is not separable into simpler single-particle equations because of the interaction term Û.

Here, at the heart of DFT, two Hohenberg-Kohn theorems provide a way to systematically map the many-body problem with $\hat{U}$, onto a single-body problem without $\hat{U}$. The first H-K theorem demonstrates that the ground state properties of a many-electron system are uniquely determined by an electron density that depends only on 3 spatial coordinates. It lays the groundwork for reducing the many-body problem of N electrons with 3N spatial coordinates to 3 spatial coordinates, through the use of functionals of the electron density. The second H-K theorem defines an energy function for the system and proves that the correct ground state electron density minimizes this energy functional. The derivation and formalism for the H-K theory is shown as follows. In DFT, the key variable is the particle density n(r)

which for a normalized Ψ is given by:

$$n(\vec{r}) = N \iiint d^3r_2\, d^3r_3 \dots d^3r_N \Psi^*(\vec{r}, \vec{r_2}, \dots \vec{r_N})\Psi(\vec{r}, \vec{r_2}, \dots \vec{r_N}) \quad (3.7)$$

The relation of equation 3.3 can be reversed, i.e. for a given ground-state density $n_0(r)$ it is possible, in principle, to calculate the corresponding ground-state wavefunction Ψ_0. In other words, Ψ_0 is a unique functional of n_0, [54]

$$\Psi_0 = \Psi[n_0] \quad (3.8)$$

and consequently the ground-state expectation value of an observable O is also a functional of n_0

$$[n_0] = \langle \Psi[n_0] | \hat{O} | \Psi[n_0] \rangle \quad (3.9)$$

In particular, the ground-state energy is a functional of n_0

$$E_0 = E[n_0] = \langle \Psi[n_0] | \hat{T} + \hat{U} + \hat{V} | \Psi[n_0] \rangle \quad (3.10)$$

where the contribution of the external potential $\langle \Psi[n_0] | \hat{V} | \Psi[n_0] \rangle$ can be written explicitly in terms of the ground-state density n_0

$$V[n_0] = \int V(\vec{r})\, n_0(\vec{r}) d^3r \quad (3.11)$$

More generally, the contribution of the external potential $\langle \Psi | \hat{V} | \Psi \rangle$ can be written explicitly in terms of the density n(r),

$$V[n] = \int V\,(\vec{r})\,n\,(\vec{r})\,d^3r \qquad (3.12)$$

The functionals T[n] and U[n] are called universal functionals, while V[n] is called a nonuniversal functional, as it depends on the system under study. Having specified a system, i.e., having specified V, one then has to minimize the functional

$$E[n] = T[n] + U[n] + \int V\,(\vec{r})\,n\,(\vec{r})\,d^3r \qquad (3.13)$$

with respect to n(r), assuming one has got reliable expressions for T[n] and U[n]. A successful minimization of the energy functional will yield the ground-state density n_0 and thus all other ground-state observables.

The variational problems of minimizing the energy functional E[n] can be solved by applying the Lagrangian method of undetermined multipliers.[14] First, one considers an energy functional that doesn't explicitly have an electron-electron interaction energy term,

$$E_s[n] = \langle \Psi_s\,[n] | \hat{T} + \hat{V_s} | \Psi_s\,[n] \rangle \qquad (3.14)$$

where T denotes the kinetic energy operator and V is an external effective potential in which the particles are moving. Thus, one can solve the so-called Kohn-Sham equations of this auxiliary non-interacting system.

$$\left[-\frac{\hbar^2}{2m}\nabla^2 + V_s\,(\vec{r}) \right] \varphi_i(\vec{r}) = \varepsilon_i \varphi_i(\vec{r}) \qquad (3.15)$$

3.3.2 Making DFT practical

The major problem with DFT is that the exact functional for exchange and correlation are not known. The functional is not known. The value of the functional for a uniform density n(r) = n_0 is known. However, approximations exist which permit the calculation of certain physical quantities quite accurately and make the DFT practical. In physics the most widely used approximation is the local-density approximation (LDA), [15] where the functional depends only on the density at the coordinate where the functional is evaluated:

$$E_{XC}^{LDA}[n] = \int \varepsilon_{XC} \ (n)n(\vec{r})d^3r \qquad (3.16)$$

The LDA turned out to be computationally convenient and robust. In the LDA, the exchange-correlation energy is taken from the known results of the many-body electron interactions in an electron system of constant density. The LDA amounts to the following picture: at each point in a molecule or solid there exists a well-defined electron density; it is assumed that an electron at such a point experiences the same many-body response by surrounding electrons as if the density of these surrounding electrons had the same value throughout the entire space as at the point of the reference electron. The exchange-correlation energy of the total molecule or solid is then the integral over the contributions from each volume element. It should be noted here that LDA is known to underestimate the band gap value in semiconductors and insulators. Because the valence and conduction band dispersions are less affected by the LDA feature, often a so-called "scissors" operator is used to push the conduction band up so that the band gap corresponds to experimental value.

Thus, real systems, such as atoms, molecules, clusters and solids, are simultaneously inhomogeneous (the electrons are exposed to spatially varying electric field produced by the nuclei) and interacting (the electrons interact via the Coulomb interaction). The way density-functional theory in the local-density approximation, deals with this inhomogeneous many-

body problem is by decomposing it into two simpler (but still highly nontrivial) problems: the solution of a spatially homogeneous interacting problem (the homogeneous electron liquid) yields the uniform exchange energy, and the solution of a spatially inhomogeneous noninteracting problem (the inhomogeneous electron gas described by the KS equations) yields the particle density. Both steps are connected by the local-density potential (16), which shows how the exchange energy of the uniform interacting system enters the equations for the inhomogeneous noninteracting system. The particular way in which the inhomogeneous many-body problem is decomposed, and the various possible improvements on the LDA are behind the success of DFT in practical applications of quantum mechanics to real materials.

3.3.3 Evolution of DFT method

Prior to the developments of DFT, the calculation of energy band structures for crystalline solids had become the major goal of computational solid state physics. In computational solid states physics, total energy calculations as a predictive tool for crystal structures and elastic properties of solids came into general use only in the mid to late 1970's. [17]

By 1970, DFT had become a widely accepted many-body approach for first principles calculations on solids. [17] Initially, energy band structure methods such as the augmented plane wave (APW) method and the KKR method were very tedious since the system of equations to be solved in each iterative step of self-consistency procedure were nonlinear.[18] Furthermore, the computer hardware at that time was limited in processor speed, but perhaps even more by memory size. A major step forward was the introduction of linearized methods, especially the linearized augmented plane wave (LAPW) and the linearized muffin-tin orbital (LMTO) method. [19] In this research work, the LMTO method is employed and the following part will introduce this method in some details. By 1980, computational solid state physicists worked on the formulation of all-electron self-consistent

methods without muffin-tin shape approximations, such as the full-potential linearized augmented plane wave (FLAPW) method with total energy capabilities. [20] In the following decades, the methods based on DFT have been proved surprisingly successful in the academic field.

Thus, calculations based on density functional theory can be used to predict physical behavior of solids that originates from the nature of atomic bonding; and quantities such as electronic structure can be studied from a fundamental perspective. DFT opens a new door to innovative research on materials across physics, chemistry, materials science, surface science, and nanotechnology, and extending even to earth sciences and molecular biology. [21] This fascinating theory, which has been employed as a basic research methodology, provides a convincing and complete theoretical system for this investigation of TCOs.

3.4 References:

[1]   S. Das and K. K. Chattopadhyay, 2016, 3, 83–103.

[2]   B. D. Culity and S. R. Stock. Elements of X–ray diffraction. Prentice Hall, New Jersey, 3 edition, 2001

[3]   M. J. Burger. X ray Crystallography. John Wily and Sons, New York, 3 edition 1962.

[4]   B.G Streetman. Solid state electronics devices. Prentice Hall of India Pvt. Ltd, New York, 1995

[5]   J. Bardeen, F. J. Blatt and L. H. Hall, editors. Proc of Photoconductivity Conf., Atlantic city, 1954. J. Wiley and Sons.

[6]   C. R. Brundle, C. A. Evans and S. Wilson. Encyclopedia of materials characterization. Reed Publishing, USA, 1992.

[7]   M. Watt. The principle and practice of electron microscopy. Cambridge Ini press, Cambridge, 1997, D. K. Schroder. Semiconductor material and device characterization. Willy Interscience, New York, 1998.

[8]   Gardiner, D.J. (1989). Practical Raman spectroscopy. Springer–Verlag. ISBN 978-0-387–50254–0, D. R. Vij. Luminescence of solids. Plenum Press, New York, 1998.

[9]   C. N. Banwell and E. M. McCash. Fundamentals of molecular spectroscopy. Tata McGraw Hill, 4th edition, 1994, Klingshirn, C. F. (2006). Semiconductor Optics. Springer. ISBN 978–3540383451.

[10] J. M. Seminario (Ed.), Recent Developments and Applications of Modern DFT, Elsevier, Amsterdam, 1996.

[11] K. Schwarz, P. Blaha, G. K. H. Madsen,Comp.Phys.Commun.147, 71-76, 2002.

[12] P. Hohenberg and W. Kohn, Phys. Rev. 136, B864, 1964.

[13] H. Eschrig, The Fundamentals of Density Functional Theory, Teubner, Leipzig, 1996.

[14] D. Joulbert (Ed.), Density Functionals: Theory and Applications, Springer Lecture Notes in Physics Vol. 500, 1998.

[15] C. Fiolhais, F. Nogueira and M. Marques (Eds.), A Primer in Density Functional Theory, Springer Lecture Notes in Physics Vol. 620, 2003.

[16] R. O. Jones and O. Gunnarsson, Rev. Mod. Phys. 61, 689, 1989.

[17] M. Levy, Phys. Rev. A 26, 1200, 1982.

[18] O. K. Andersen and T. Saha-Dasgupta, Phys. Rev. B 62, 16219, 2000.

[19] E. Zurek, O. Jepsen and O. K. Andersen, Chem.Phys.Chem. 6, 1934, 2005.

[20] E. Wimmer, H. Krakauer, M. Weinert and A. Freeman, J, Phys. Rev. B 24 864, 1981.

[21] W. Koch and M. C. Holthausen, A Chemist's Guide to Density Functional Theory, John Wiley & Sons, New York, 2001.

CHAPTER 4:

SYNTHESIS AND BASIC CHARACTERISATION OF SIZE MODULATED Fe$_3$O$_4$ NANOPARTICLES

Abstract

Magnetite (Fe_3O_4), a relaxor multiferroic material, has attracted much attention in the last decade due to the recent understandings of charge-ordering phenomena below Verwey transition and uncountable potential biomedical applications. Highly water dispersible spherical Fe_3O_4 nanoparticles (NP's) with enormous variation in size (13 - 236 nm) had been synthesized by a facile solvothermal approach using disodium tartrate and polyethelene glycol as crystal grain growth inhibitor and stabilizer in polyol medium. By controlling the concentration of surfactants, size-distribution of nanoparticles was controlled. Williamson-Hall analysis was employed to evaluate the maximum grain-size of the as-synthesized powder-samples. Average particle-size was also verified from a voigt fit of size-distribution obtained from FE-SEM micrographs, which revealed a close estimation with respect to the W-H grain-size. A thorough XPS analysis was employed to determine the difference in binding energies of the tetrahedral and octahedrally co-ordinated Fe atoms along with degree of stoichiometry and related surface-chemistry. The non-stoichiometry factor (δ) was found independent of particle-size, which resulted a spontaneous non-stoichiometry, common in most multivalent transition metal oxides. In addition, these Fe_3O_4 NP's may be useful in other fields, such as hyperthermia treatment of cancer and targeted drug delivery because of their size-dependent magnetic property and excellent stability.

4.1. Introduction

The oldest known magnetic material Magnetite (Fe_3O_4) has attracted much attention in the last decade due to the recent understandings of charge-ordering phenomena in low-temperature symmetries during Verwey transition and associated relaxor properties along with uncountable potential biomedical applications such as biomolecular separation, biological sensing & cell tracking, targeted drug delivery, magnetic fluid hyperthermia (MFH) treatment of tumour cells, gene delivery, waste water purification, environmental remediation, nickel–ion batteries and magnetic resonance imaging (MRI) as T_2 contrast agents. Among various magnetic materials, Fe_3O_4 NP's have been extensively investigated due to their excellent biocompatibility, negligible toxicity and tunable magnetic property. For spherical particles, the surface area to volume ratio is inversely proportional to the radius, so a substantial reduction in particle size leads to a dramatic increase in surface area and thereby the surface-energy term and associated defect-states; giving rise to certain physio-chemical properties.

There exist roughly 16 different iron oxide & oxyhydroxide polymorphs having a wide range of properties and performance in various environments. Among these, three most common and important iron oxide polymorphs are hematite (α-Fe_2O_3), maghemite (γ-Fe_2O_3), and magnetite (Fe_3O_4). Magnetite NP's exhibit unique size-dependent magnetic properties. Bulk magnetite crystallizes in the inverse cubic-spinel structure$(Fe^{3+})_A[Fe^{2+}Fe^{3+}]_B(O^{2-})_4$; space group O_h^7 (Fd3m) and lattice parameter$a_c = 8.407$ Å, which consists of face-centred cubic (FCC) close-packed lattice of O^{2-} ions. Magnetite possesses a smaller unit cell than hematite and is free of vacancies unlike maghemite. There are two types of Fe atoms: the tetrahedrally coordinated A-sites (Wyckoff site 8a, point group $\bar{4}$3m) and the octahedrally coordinated B-sites (Wyckoff site 16d, point group $\bar{3}$m) with respect to the oxygen sublattice. Rapid hopping of an extra down-spin electron between B sites results in minority-spin-polarized electronic conductivity ascribing its half-metallic behaviour at room-temperature. In fact, Fe_3O_4 possesses a conducting minority spin channel and semiconducting majority spin channel, which results an absolute spin polarization at the Fermi level, making magnetite a prospective material for spintronic devices too.

Basically, magnetic properties of bulk magnetite with a multidomain structure are governed by two distinct mechanisms. The first is the anti-ferrimagnetic super-exchange interaction between the Fe_{Oct}^{3+} and Fe_{Tet}^{3+} sites coupling through the overlapping 2p orbital of intermediate

oxygen. Association of B-sites in a pyrochlore lattice with corner-sharing tetrahedra gives rise to a magnetic moment antiparallelly aligned with A-sites having unequal magnitude. The second factor is the predominant double-exchange interaction between the Fe_{Oct}^{2+} and Fe_{Oct}^{3+} sites via hopping of spin-down electrons, which makes them align parallel. Therefore, all the Fe_{Oct}^{2+} ions contribute to the magnetic moment, while all Fe^{3+} ions cancel each other out. In fact, there are twice as many B-site Fe^{3+} $3d^5$ ($S = {}^5/_2$) up-spins as there are down-spins at the A-sites, resulting a net non-vanishing magnetic moment, giving rise to ferrimagnetism with a Curie temperature of 858 K.

As the particle-size decreases below ~100 nm, the particles tend to attain a single-domain structure, where coercivity is maximized and Curie temperature gets lowered. When the particle size is smaller than ~20 nm, the magnetization of magnetite NP's is randomized by thermal agitation. As a consequence, they become superparamagnetic with only 2 stable orientations. The temperature below which a particle becomes superparamagnetic i.e., attains a steeper magnetization curve with large susceptibility and zero hysteresis area, is called the blocking temperature (T_B) and can be calculated from $T_B = {}^{KV}/_{25k_B}$, where K is the magnetic anisotropy energy density, k_B is the Boltzmann constant, and V is the average volume of the NP's. NP's with sizes of 3−100 nm have garnered a great deal of attention from the perspective of both basic and developmental sciences in a distinct variety of fields. This is due to the fact that these NP's exhibit size-dependent electrical, optical, magnetic, and catalytic phenomena that cannot be realized by their bulk counterparts.

Quantum dots (QD) are effectively zero-dimensional semiconducting nanocrystals with typical size range ~ 1-10 nm, that exhibit quantum confinement of the electronic states, due to extreme limitations in size. QD's not only achieve a change in lattice parameters, compared to the bulk materials, but also lose long-range interactions unless explicit dense-packing. Two typical types viz., (i) colloidal QD's and (ii) QD's directly nucleated inside a host matrix (generally a mesoporous nanonetwork or a thin film). Colloidal QD's are advantageous for attaining a very narrow size distribution, which results in well-defined optoelectronic properties in terms of absorption excitonic peaks and photoluminescence. In this work, a microwave-assisted one-step synthesis of Fe_3O_4 NP's in polyol medium has been performed with a size-variation from quantum regime to bulk order to reinvestigate increment in optical band-gap and phonon confinement effects probed by red-shifting and asymmetric Raman line-shape.

4.2 Experimental Section

4.2.1 Introduction

Hydrothermal or solvothermal method is one of the most common and effective synthetic routes to fabricate the nanomaterial with a variety of morphologies. In this method, the reactants are placed intoan autoclave filled with water or organic compound to carry out the reaction under high temperature and pressure conditions. If the nonaqueous solvents are utilized as reaction medium, it is termed as solvothermal method; whereas, in case the preparation is carried out in the presence of water, it is known as hydrothermal process (Cushing et al., 2004; Wu et al., 2002). Different kinds of autoclaves and their functions are deeply discussed in the literature (Hakuta et al., 2005; Rabenau, 1985). Generally, Teflon-lined autoclaves are capable of working at high temperature and pressure. In addition, it sustains alkaline media and exhibits a strong resistance to hydrofluoric acid when compared to glass and quartz autoclaves. Therefore, Teflon-lined autoclave is chosen as an ideal container to perform the reaction under desired conditions. Precise control in hydrothermal process is the key factor that enables the synthesis of various nanostructured inorganic materials (Shi et al., 2013). This method can facilitate and accelerate the reaction among the reactants, promote hydrolysis, followed by crystal growth resulting in self-assembly of nanomaterials in the solution. Moreover, the properties, morphology, size, and structure of nanomaterials can be tailored easily by varying the different reaction parameters, such as reaction time, temperature, reaction medium, pressure, pH, and concentration of the reactants and filled volume of autoclave. This method can be suitable for the preparation of nanomaterials with a variety of shapes as compared to other methodologies.

4.2.2 Reagents and materials

All reagents were of analytical grade (Assay $\geq$ 99%) and used directly without any further purification. Ethylene glycol (EG), diethylene glycol (DEG) and polyethelene glycol (PEG; Avg. mol. wt. ~ 6000) were used to prepare the polyol solvent. Ferric Chloride hexahydrate (FeCl$_3$. 6H$_2$O) and anhydrous sodium acetate (CH$_3$COONa) with $\geq$ 99.5% purity are the principle precursors, purchased from SIGMA-ALDRICH. Hydrated disodium (+) tartrate [(CHOH . COONa)$_2$. 2H$_2$O] was bought from LOBA Chemie. Absolute ethanol from Merck and deionised water (~18.2 MΩ) were used for washing.

4.3 Synthesis Procedure

4.3.1 Solvothermal Method

Fe_3O_4 nanoparticles (NP's) of different size have been prepared by a traditional one-step solvothermal approach. In a typical synthesis of 47 nm Fe_3O_4 NP's 1.50 gm (5.55 mmol) $FeCl_3$. $6H_2O$ was first mixed vigorously in a mixture of 40 mL ethylene glycol and 40 ml diethylene glycol to form a clear solution. Then, 0.35 gm (1.52 mmol) hydrated disodium (+) tartrate was added followed by 3.00 gm (36.57 mmol) of anhydrous sodium acetate and 3.5 gm (0.58 mmol) polyethelene glycol (mol. wt. = 6000). Then, this mixture was ultrasonicated for 10 minutes and magnetically stirred for an hour at 80°C to form a homogeneous dark yellow solution. Thereafter the resulting solution was put into a teflon-lined stainless steel-autoclave with 100 mL capacity and maintained at 185°C for 14 hrs. After natural cooling, the black product was precipitated with ethanol followed by thorough centrifugation, washing (in deionized water & ethanol) and vacuum-drying at 65°C to acquire fine magnetite powder. The amount of disodium tartrate and PEG-6000 was varied in between 0.05-0.65 gm and 3-4 gm respectively to tune particle-size, which obstruct crystal grain growth and act as stabilizer. Commercial Fe_3O_4 powder was also purchased from SIGMA-ALDRICH to compare the properties of as-synthesized NP's.

Table 4.1: Composition of reagents in different sample

Sample Code	Amount of reagents					
	EG (ml)	DEG (ml)	$FeCl_3$. $6H_2O$ (gm)	Sodium tartrate (gm)	Sodium acetate (gm)	PEG -6000 (gm)
S1	40	40	1.50	0.05	3.00	3.00
S2				0.20		3.25
S3				0.35		3.50
S4				0.50		3.75
S5				0.65		4.00

4.3.2 Role of surfactants and capping agents in coating mechanism

In the synthesis and storage of multivariant transition metal oxides; stability demands utmost importance. On exposure to ambient atmosphere, the surface of Fe_3O_4 crystallites are often covered with a few layers of α-Fe_2O_3 (as is true for most oxides), monolayer amounts of surface hydroxyls as well as physiosorbed H_2O. Very often organic compounds are employed to passivate the surface of NP's during or after synthesis to avoid agglomeration. The main cause is the hydrophobic surfaces with a large surface area-to-volume ratio, which in absence of a suitable surface-coating, acquires hydrophobic interactions in between causing interparticle aggregation and formation of large clusters. The capping agents limit the size of NP's by preventing further particle growth and agglomeration during synthesis and can also be useful in controlling the particle reactivity, imparting solubility and packing characteristics. Surfactants are also used to control morphology and protect nanoparticles from deteriorating in environment.

In this reaction, sodium acetate acts as a nucleating agent and helps to partially reduce Fe^{3+} ions to Fe^{2+} in the polyol medium to form Fe_3O_4. PEG not only functionalizes the surface of NP's and acts as a stabilizer, but also dissipates heat energy from microwave to facilitate the reaction. Biocompatible sodium tartrate was chosen, as it can act as a crystal grain growth inhibitor depending on concentration for the synthesis of ultra-small nanoparticles and QD. In addition, the two carboxylate groups of tartrate salts have strong coordination affinity to Fe^{3+} ions. This supports the attachment of tartrate groups on the surface of the Fe_3O_4 NP's, controlling growth. Hence, the as-synthesized NP's are also intrinsically stabilized with a layer of the hydrophilic ligands in situ, preventing them from aggregating into larger crystals, which is essential for their long-term stability in aqueous media. Besides, tartrates, found in fruits like grapes, tamarind etc are completely biocompatible and non-toxic and hence ideal for biomedical applications. The joint effect of PEG & tartrate ions to form a core-shell structure in increasing solubility and stability in aqueous medium have been elaborated schematically.

4.4 Characterization techniques

4.4.1 X-ray diffraction (XRD) & Williamson-Hall analysis

The crystallographic phase composition of the as-synthesized samples was determined from X-ray diffraction using Rigaku Miniflex powder X-ray diffractometer; operated at 40kV-15mA. Data was acquired in a 2θ range: 15°-80° in steps of 0.02° at a rate 1°/min. All the diffraction peaks are indexed ac. to the inverse-spinel structure known for the Fe_3O_4 crystal (JCPDS card no. 85-1436) and no additional peaks were detected, confirming pure phase material. In addition, the average grain-size (d_{WH}) and strain (ε) were calculated from the Williamson-Hall equation considering spherical morphology:

$$\beta \cos \theta = 4\varepsilon \sin \theta + {0.89\lambda}/{d_{WH}}$$

where β is the full width at half-maximum (FWHM) of a Bragg-peak, θ is the diffraction-angle and $\lambda = 1.5406\text{Å}\ (for\ Cu\ k_\alpha\ line)$. Depicting $\beta \cos \theta$ vs $\sin \theta$ plot, d_{WH} and ε were respectively calculated from the intercept and slope of the straight line. The regular increase in FWHM with decreasing particle-size can be observed clearly in figure-II as a result of increase in tensile stress, point-defects at the surface and an overall disorder in the nanocrystals. The values of d_{WH} have been listed in Table-IA and IB for all the samples.
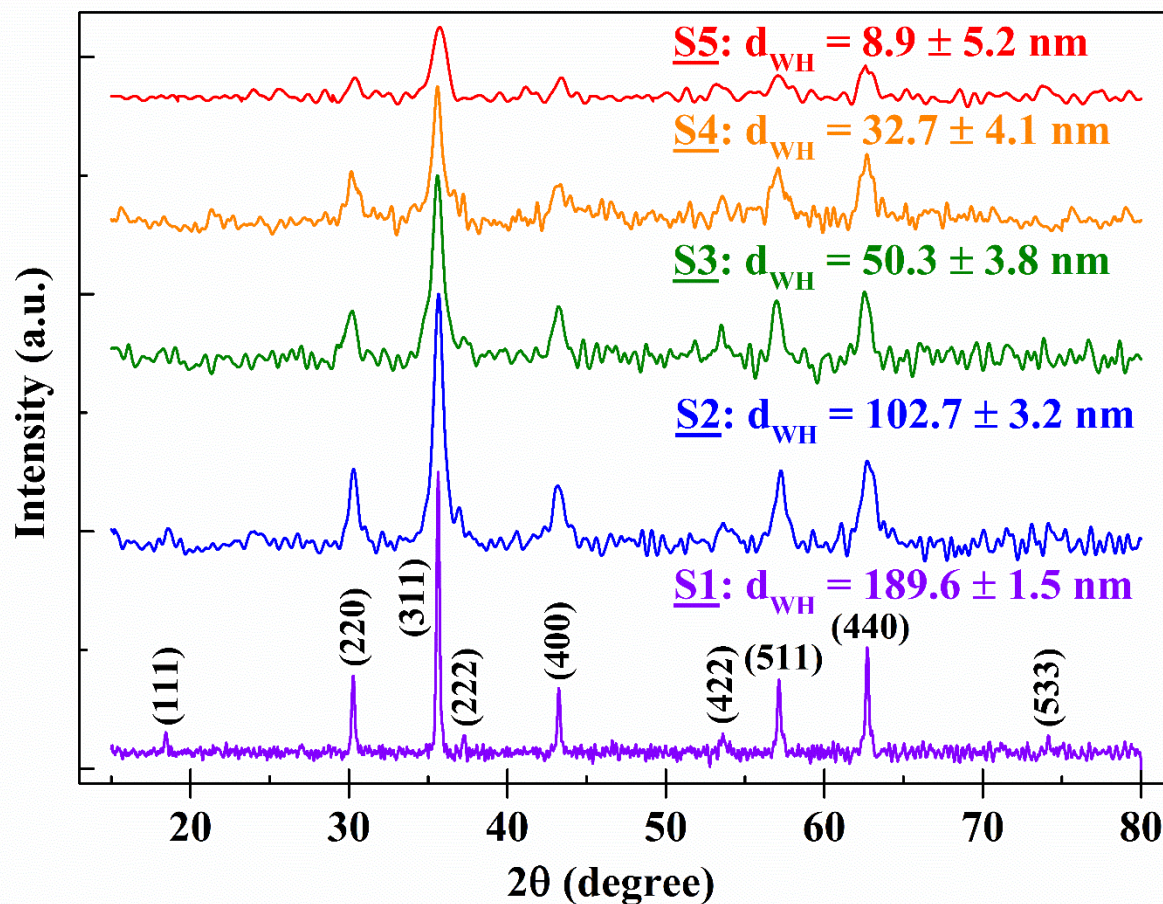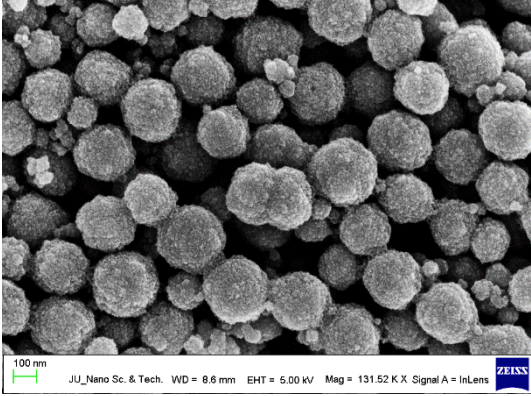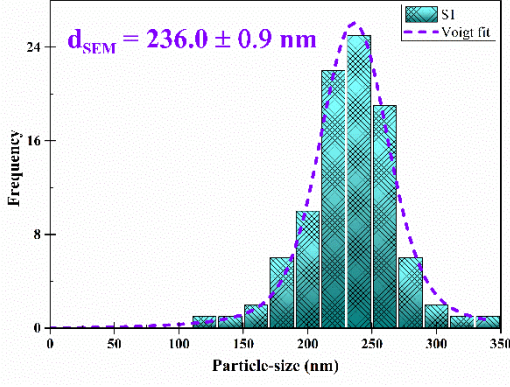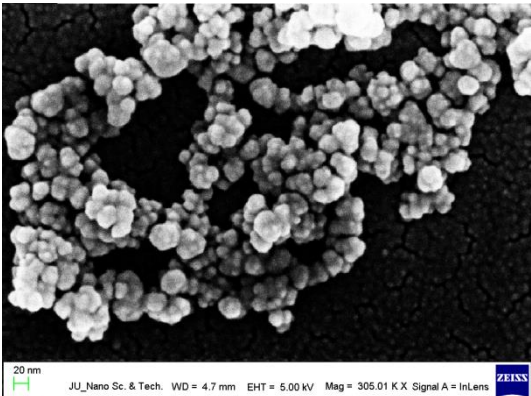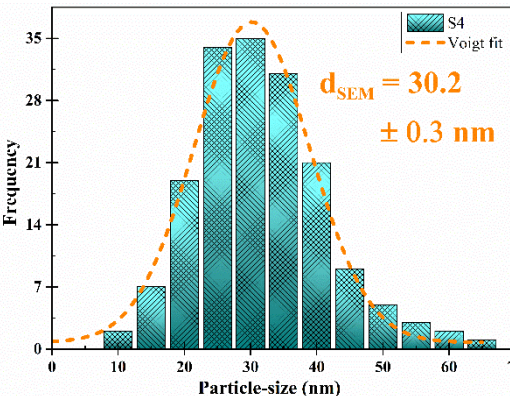
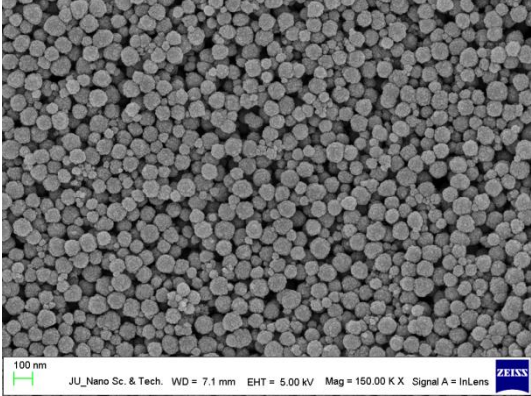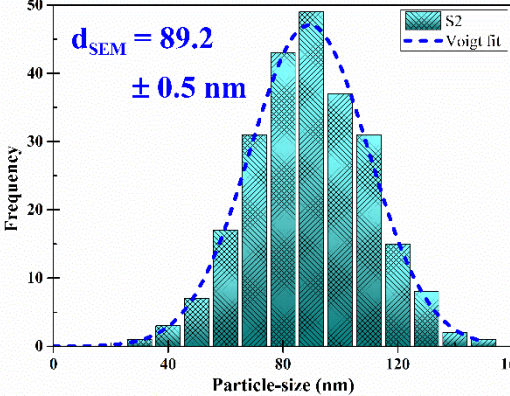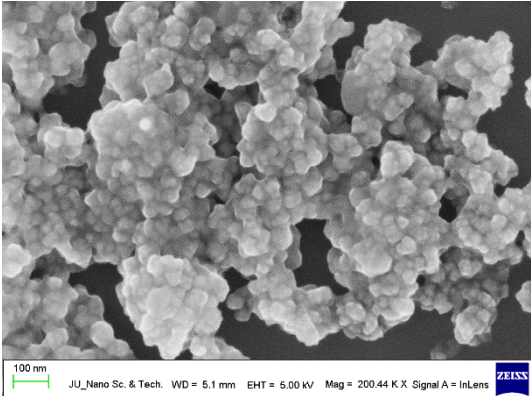**Fig 4.2: XRD pattern of samples**

4.4.2 Field Emission Scanning Electron microscopy (FE-SEM)

Surface morphology and size-distribution of NP's were analysed using a field emission scanning electron microscope (FESEM, JEOL 6340F FEG-SEM), whereas a high-resolution transmission electron microscope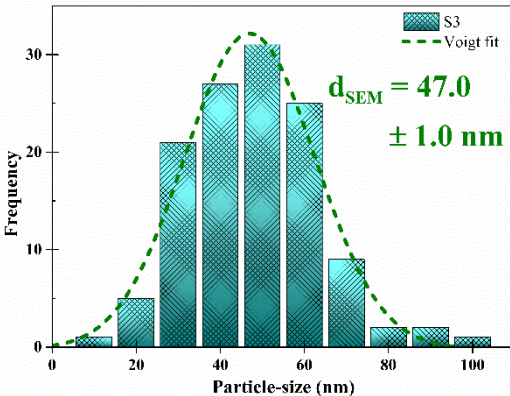 (HRTEM, JEOL-JEM 2100) operated at 200 kV; was employed to observe the NP's, analyse crystalline nature & unidirectional growth. The polycrystalline samples got a spherical morphology because of the polyol medium and tartrate ions. The regular decrease in size and increase in monodispersity can be observed.

Sample-code	FE-SEM Micrograph	Size-distribution
S1		$d_{SEM} = 236.0 \pm 0.9$ nm
S2		$d_{SEM} = 89.2 \pm 0.5$ nm
S3		$d_{SEM} = 47.0 \pm 1.0$ nm
S4		$d_{SEM} = 30.2 \pm 0.3$ nm
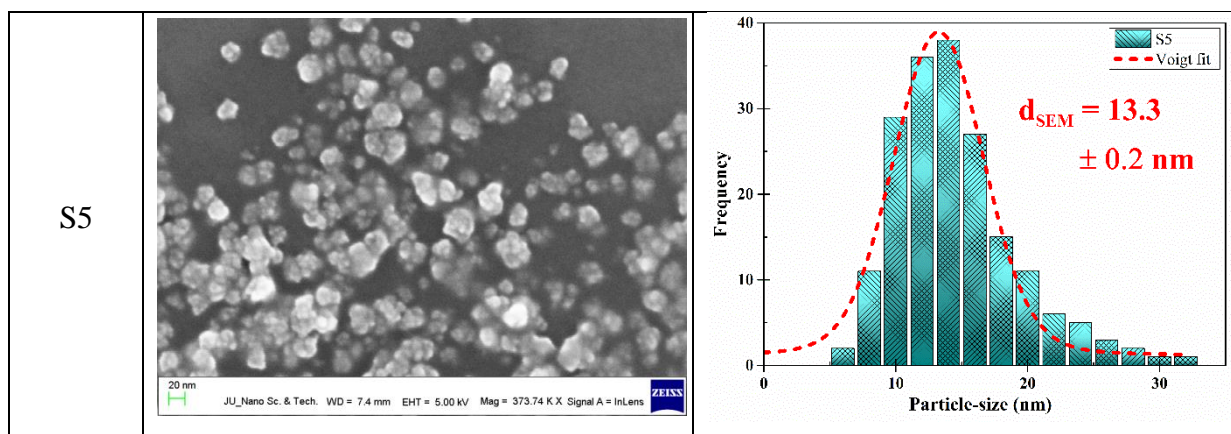
Fig 4.3: FE-SEM Micrographs and Frequency Distribution graph with Particle Size

4.4.3 Fourier-transform infrared (FT-IR) spectroscopy

The coordinative effect of carboxylate groups in the surface-composition was further verified by FT-IR spectra, collected from Shimadzu FTIR-8400S. The spectra showed characteristic absorption peaks at 581 and 1370 cm^{-1} due to Fe-O bending and stretching vibrations respectively. The peak at 979 cm^{-1} is assigned to the bending vibrations of =C-H and C-C-O groups, whereas the 1083 cm^{-1} peak is due to CO-C axial deformation and aliphatic bending vibrations of C-C-H groups. The peaks at 1598 and 1685 cm^{-1} are attributed to –COO-stretching, bending vibrations of water molecules absorbed on the surface of Fe_3O_4 NP's and C=O stretching. The symmetric and asymmetric stretching of the methylene (=CH$_2$) group and C-H stretching caused peaks at 2888 and 2987 cm^{-1}. Finally, the bands at 3430 and 3733 cm^{-1} appeared due to the stretching and bending vibrations of the -OH groups, which are also the characteristic peaks of PEG-6000. Hence, the FT-IR spectra confirms the successful formation of tartrate coated-PEGylated Fe_3O_4 NP's.

4.5. Conclusion:

In conclusion, we have demonstrated controlled UDR-like (Universal Debye Relaxation) NC dispersion in a series of highly mismatched ZnO/*Ch* lattices by tuning the delocalization of minority carriers. Doping induced quasi Fermi levels are considered to be playing an important role in terms of and under the influence of . In this context, trap mediated carrier recombination is the key part determining the overall sign of dielectric capacitance. This study points to a novel scope for generating NC in anion substituted metal oxide semiconductors, which constitute a

significant portion of contemporary electronics in terms of photovoltaics and new solar cell materials. In a time when the Si-based solar cell technology is fast approaching its theoretical limit; abundant, environment friendly and band engineered is a strong candidate as a source to harvest alternative energy. Fundamental aspects of NC as well as device applications can be triggered upon further experimental venture.

4.5. References:

[1] T. Noguchi, M. Kitagawa, and I. Taniguchi, Jpn. J. Appl. Phys. **19**, 1423 (1980).

[2] J. Wu *et. al.*, IEEE Electron Device Lett. DOI: **10.1109/LED.2018.2810203**.

[3] A. G. U. Perera, W. Z. Shen, M. Ershov, H. C. Liu, M. Buchanan and W. J. Schaff, Appl. Phys. Lett. **74**, 3167 (1999).

[4] T. J. Phillips and N. T. Gordon, J. Electron. Mater. **25**, 1151 (1996).

[5] J. Shulman, Y. Y. Xue, S. Tsui, F. Chen, and C. W. Chu, Phys. Rev. B **80**, 134202 (2009).

[6] C. C. Wang, G. Z. Liu, M. He, and H. B. Lu, Appl. Phys. Lett. **92**, 052905 (2008).

[7] M. Ting, R. dos Reis, M. Jaquez, O. D. Dubon, S. S. Mao, K. M. Yu, and W. Walukiewicz, Appl. Phys. Lett. **106**, 092101 (2015).

[8] Ch. D. Wagner, A. V. Naumkin, A. Kraut-Vass, J. W. Allison, C. J. Powell, and Jr. J. R. Rumble, NIST Standard Reference Database 20, Version 3.4.

[9] G. Eda, H. Yamaguchi, D. Voiry, T. Fujita, M. Chen, and M. Chhowalla, Nano Lett. **11**, 5111, (2011).

[10] H. F. Franzen, M. X. Umana, J. R. McCreary, and R. J. Thorn, J. Solid State Chem. **18**, 363 (1976).

[11] Som S and Sharma S K, J. Phys. D: Appl. Phys. **45**, 415102 (2012).

[12] G. Oster, A. Perelson, and A. Katchalsky, Nature, **234**, 393 (1971).

[13] J. Jamnik, and J. Maier, Phys. Chem. Chem. Phys., **3**, 1668 (2001).

[14] Wang Y, Chen J, Dong L, and Ma D, J. Appl. Phys. **114**, 113703 (2013).

CHAPTER 5:

NEGATIVE CAPACITIVE (NC) SWITCHING IN SIZE-MODULATED MAGNETITE (Fe$_3$O$_4$) NANOPARTICLES

Abstract

A persistent low-frequency negative capacitance (NC) dispersion has been detected in half-metallic magnetite (Fe_3O_4) nanoparticles having a size-variation: 13-236 nm; under application of moderate positive DC bias, probed via impedance spectroscopy. A 3D Cole-Cole plot fitting technique has been used employing Harvriliak-Negami model to recapitulate the relaxation time (τ) of the associated oscillating dipoles, related shape-parameters (α,β) and resistivity for different sizes. Universal Debye relaxation (UDR) theory requires a modification to deal with the shifted static NC-dispersion plane in materials showing both +ve and –ve capacitance about a transition-frequency (f_0). A generalized dispersion-formula has been proposed in this regard to fit the complete data of +ve and –ve capacitance regime including the diverging transition-point. In addition, a comprehensive model has been discussed to differentiate the continuous transition from –ve to +ve capacitance due to localized charge recombination and capacitive switching. A consistent blue-shift of 'f_0' was observed with increasing external electric field and decreasing particle-size. An inherent non-stoichiometry due to iron-vacancies [$Fe_{3(1-\delta)}O_4$] detraps holes and builds up p-type nature, which consequently gives rise to more covalent and heavier dipoles slowing down the Maxwell-Wagner interfacial polarization dynamics. This combinational effect has been apprehended for the sluggish response of associated dipoles and stabilization of NC.

5.1 Introduction:

So far, negative capacitance (NC) phenomena have been an exclusive paradigm of contemporary research, detected in an extensive variety of fields and materials such as ferroelectric nanostructures, thin films, amorphous chalcogenides, binary oxides, perovskites, solar cells, electrorheological fluids, organic and inorganic compounds, composites, glass alloys, semiconductor diodes, heterojunctions etc. The manifestation of stable NC dispersion is theoretically a bit adequate for ferroelectric materials, but NC in non-ferroelectric substances/devices have been explained using versatile ideas including localization of charge in trap/interface states, contact injection, extrinsic or doping effects, space-charge propagation, minority carrier injection etc. A generalized theory of NC for all the above-mentioned systems is still way too far to reach. In a series R-L-C circuit, capacitance (C) and inductance (L) compete for making the current variation to lead over and lag behind the applied voltage respectively. Positive capacitance in semiconducting or insulating materials are governed by the space-charge accumulation in the grain-grain boundary constitution causing Maxwell-Wagner interfacial polarization and Cole-Davidson theory, whereas on application of an external field; the hopping of delocalized charge-carriers to nonlinear localized sites might give rise to an inductive effect. Phenomenologically, the interpretation of current lagging behind the voltage agitation can be associated with both +ve inductance or -ve capacitance. But, the absence of considerable spontaneous magnetic field in most of the materials hardly supports the inductive origin [resulting $O(L) \sim pH$ only in standard polycrystalline pallets]. Hence, the interpretation is carried forward with the notion of negative capacitance. Another analogous current-voltage phase relationship is observed in frequency-range greater than a few tens of MHz, where inductive effects start dominating. But this outcome has nothing to do with NC. For example, in a series R-L-C circuit, reactance, $\chi = \omega L - \frac{1}{\omega C}$; so even for fixed values of C and L; at sufficiently high frequencies, inductive reactance $(\sim \omega)$ gets overestimated against the capacitive nature $\left(\sim \frac{1}{\omega} \right)$; which is known as parasitic inductance in capacitor manufacturing industries. So, true NC should not be confused with high-frequency pseudo-inductive genre.

5.2 An Overview of Iron Oxides:

Out of more than 16 polymorphs of iron oxide and oxyhydroxides; magnetite (Fe_3O_4) with an inverse spinel cubic structure (point group: Fd3m) has been the most interesting and crucial one for more than three centuries to theoretical as well as experimental condensed matter physicists and material scientists; because of its unique electrical and magnetic properties. This half-metallic and ferrimagnetic material has also been observed to act as a relaxor multiferroic upto 40K, far below the Verwey transition (120-125 K) – which is still not completely understood. Moreover, the theoretically claimed 100% spin-polarized material concerning double-exchange and super-exchange interactions; gets converted to h-Fe_3O_4 with a normal spinel lattice on application of $\geq 10 GPa$ pressure. Previously, many researchers have detected oxygen-stoichiometry, strain and grain-size to be the critical parameters, that control its electric and magnetic properties. Here we report, Fe_3O_4 also shows a frequency-dependent –ve to +ve capacitive switching; adaptable via application of external DC bias and thereby propose a probable model to explain these observations.

5.3 Experimental Section:

5.3.1 Sample Preparation:

Fe_3O_4 nanoparticles (NP's) of different size have been prepared by a traditional one-step solvothermal approach. In a typical synthesis of 47 nm Fe_3O_4 NP's 1.50 gm (5.55 mmol) $FeCl_3$. $6H_2O$ was first mixed vigorously in a mixture of 40 mL ethylene glycol and 40 ml diethylene glycol to form a clear solution. Then, 0.35 gm (1.52 mmol) hydrated disodium (+) tartrate was added followed by 3.00 gm (36.57 mmol) of anhydrous sodium acetate and 3.5 gm (0.58 mmol) polyethelene glycol (mol. wt. = 6000). Then, this mixture was ultrasonicated for 10 minutes and magnetically stirred for an hour at 80°C to form a homogeneous dark yellow solution. Thereafter the resulting solution was put into a teflon-lined stainless steel-autoclave with 100 mL capacity and maintained at 185°C for 14 hrs. After natural cooling, the black product was precipitated with ethanol followed by thorough centrifugation, washing (in deionized water & ethanol) and vacuum-drying at 65°C to acquire fine magnetite powder. The amount of disodium tartrate and PEG-6000 was varied in between 0.05-0.65 gm and 3-4 gm respectively to tune particle-size, which obstruct crystal grain growth and act as stabilizer. To investigate the dielectric response, 0.5 gm of each powder-sample was cold-pressed by applying 0.5 GPa pressure to prepare fine polycrystalline pallets of 2 mm thickness and 9.5

mm diameter and conducting silver-paste was applied in top-bottom configuration to attain capacitor geometry.

5.3.2 Impedence Spectroscopy:

5.3.2.1 Cole Cole Plot Fitting:
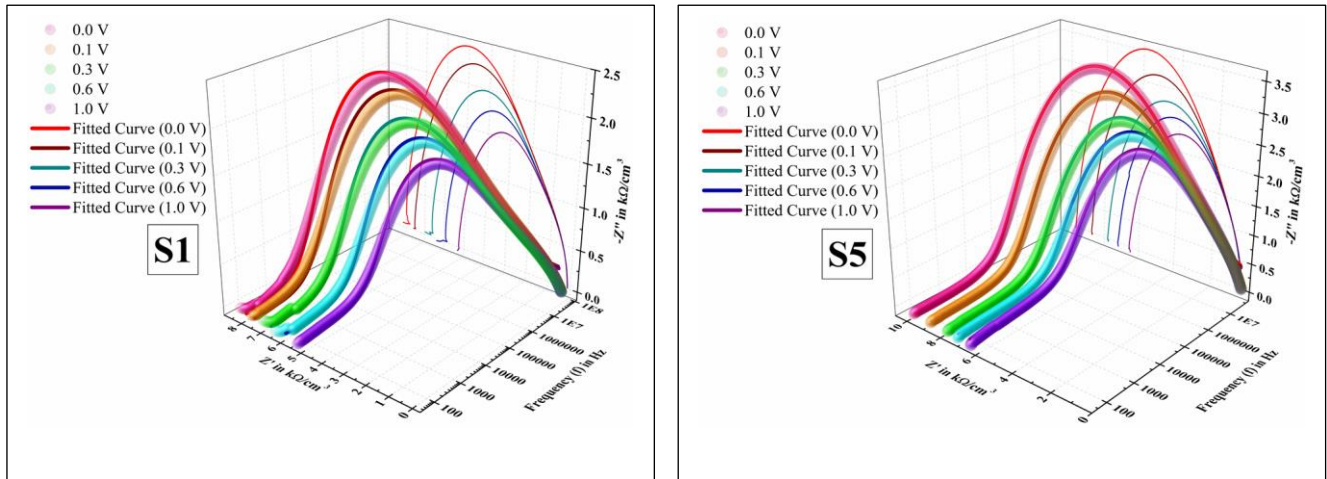
Fig 5.1: Cole-Cole plot of (a) Sample 1 (b) Sample 5

The dielectric relaxation response of an ensemble of ideal noninteracting (with respect to other dipoles and the environment) dipoles to an alternating electric field is usually expressed by the Debye relaxation (DR) formula. But, considering feasible interactions, the relaxation mechanism for symmetrically and asymmetrically broadened loss-peaks are described by the Cole-Cole & Cole-Davidson equations with exponent cum shape-parameters α & β ($0 \leq \alpha, \beta \leq 1$) respectively. These dynamics have been further merged by Harvriliak and Negami for generalization, which reduces to DR with a single relaxation time for $\alpha = 1$ & $\beta = 1$. For angular frequency; $\omega = 2\pi f$, complex permittivity $[\hat{\varepsilon}(\omega) = \varepsilon'(\omega) - j\varepsilon''(\omega), j = \sqrt{-1}]$ and its real (implies energy storage) & imaginary (implies dissipation/loss) parts can be expressed as follows:

Table 5.1: Debye Relaxation to Cole-Cole equation

Debye Relaxation	Cole-Cole equations
$\hat{\varepsilon}(\omega) = \varepsilon_\infty + \dfrac{\Delta\varepsilon}{1+j\omega\tau}$	$\hat{\varepsilon}(\omega) = \varepsilon_\infty + \dfrac{\Delta\varepsilon}{\{1+(j\omega\tau)^\alpha\}^\beta}$
$\varepsilon'(\omega) = \varepsilon_\infty + \dfrac{\varepsilon_s - \varepsilon_\infty}{1+\omega^2\tau^2}$	$\varepsilon'(\omega) = \varepsilon_\infty + \dfrac{(\varepsilon_s - \varepsilon_\infty)\cos\beta\varphi}{\left[1+2(\omega\tau)^\alpha \cos {}^{\alpha\pi}/_2 + (\omega\tau)^{2\alpha}\right]^{\beta/2}}$
$\varepsilon''(\omega) = \dfrac{(\varepsilon_s - \varepsilon_\infty)\omega\tau}{1+\omega^2\tau^2}$	$\varepsilon''(\omega) = \dfrac{(\varepsilon_s - \varepsilon_\infty)\sin\beta\varphi}{\left[1+2(\omega\tau)^\alpha \cos {}^{\alpha\pi}/_2 + (\omega\tau)^{2\alpha}\right]^{\beta/2}}$

Here, ε_s is the static (saturated) permittivity, ε_∞ gives the high-frequency limit, $\Delta\varepsilon = \varepsilon_s - \varepsilon_\infty$ is known as the dielectric strength and τ is the characteristic relaxation time of the oscillating dipoles. These formulae are also similar for analogous dielectric quantities. To understand the complete impedance response, a 3D Cole-Cole curve was plotted and fitted with the H-N equations. For all the samples, α and β varied in between 0.97-1.00 and 0.52-0.71 respectively; which imply small deviation from DR in such a half-metallic ferrite compound. In literature, ferrite materials have been seen to possess distinct grain-grain boundary resistance correlations. Their grains do have higher or almost equal resistivity compared to the grain-boundaries. The Cole-Cole curves show unclear dissociation b/w the grain and grain-boundary contributions, which reflect an identical situation. Comparing the two extreme sizes, a little higher resistivity for the smaller variant has been observed, following the general trends.

5.3.2.2 Capacitive Switching:

The DR formula for permittivity can be extended for capacitance also, as the two quantities are proportional to each other. But for materials, that exhibit both +ve and –ve values of capacitance, this formula fails to fit the experimental data. This is because of the shifting of negative static plane to a new frequency viz. f_0. Thus, to describe positive capacitance dispersion, the modified formula as follows:

$$C_+(f) = C(\infty) + \dfrac{\Delta C_+}{1+4\pi^2(f-f_0)^2\tau^2}, \qquad C(\infty) > 0, \qquad \Delta C_+ = C_{s+} - C(\infty) \to 0_+$$

Likewise, the negative capacitance dispersion can be formulated as:

$$C_-(f) = C(0) + \frac{\Delta C_-}{1 + 4\pi^2(f_0 - f)^2\tau^2}, \qquad C(0) < 0, \qquad \Delta C_- = C(0) - C_{s-} \rightarrow 0_-$$

These two formulae can be merged to evaluate the complete dispersion by considering, $|C(\infty)| \cong |C(0)| = C_0$ (as the limiting value of the phase-lead or lag acquired by the associated dipoles typically settles for the same order of magnitude) and $|\Delta C_+| \cong |\Delta C_-| = |\Delta C|$ via a step-function defined as: $\Theta(f, f_0) = -1\ for\ f < f_0\ and + 1\ for\ f > f_0$; but undefined at $f = f_0$; such as $\left.(f - f_0)\middle/ |f - f_0|\right.$. So, the proposed modification of UDR is given by:

$$C(f) = \Theta(f, f_0)\left[C_0 + \frac{|\Delta C|}{1 + 4\pi^2|f - f_0|^2\tau^2}\right]$$

By fitting the experimental data using this formula, relaxation-time (τ) has been extracted, which is found to be blue-shifted with increasing DC bias and decreasing particle-size.
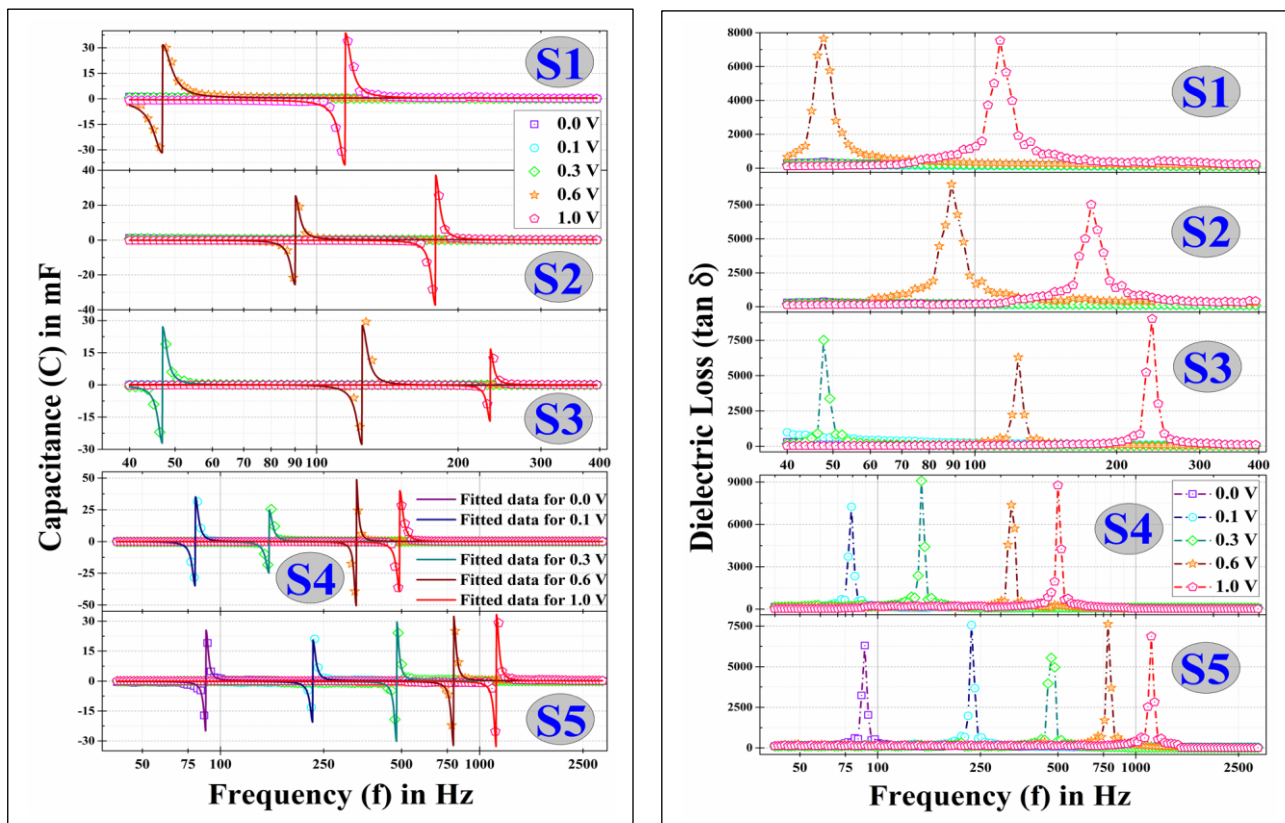

Fig 5.2: (a)Capacitance vs Frequency plot, (b) Dielectric vs Frequency plot

5.3.2.3 Dielectric Loss Dispersion:

On the other hand, dielectric loss-tangent [$\tan\delta = {\varepsilon''(\omega)}/{\varepsilon'(\omega)}$] exhibits subsequent delta functions at the transition-frequencies.

5.4 Results and Discussion:

5.4.1 Heavy Dipole Dynamics:

The inner dynamics of the NC associated dipoles can be well-explained by the phasor-diagram schematics shown on Figure-4(b). Let $\overrightarrow{OA}$ be the current vector ($\vec{I}$). The system possesses resistive, capacitive and inductive components due to grain & grain-boundary contributions, Maxwell-Wagner interfacial polarization and non-linear hopping of charge-carriers respectively. It also got some NC-effects, for the spontaneous non-stoichiometry present in Fe_3O_4.

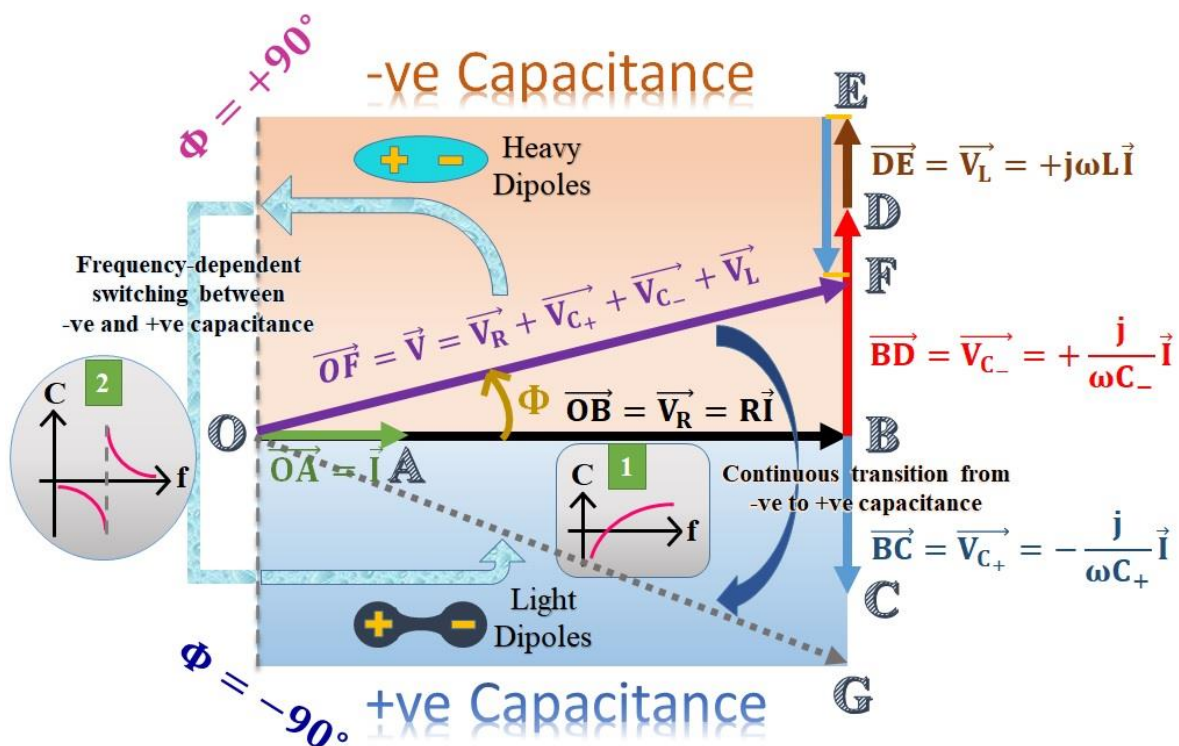**Fig 5.3: Phasor Diagram of Heavy Dipole Dynamics**

Let, the corresponding voltage vectors be $\overrightarrow{V_R}$, $\overrightarrow{V_L}$, $\overrightarrow{V_{C+}}$ and $\overrightarrow{V_{C-}}$ represented by the lines $\overrightarrow{OB}$, $\overrightarrow{DE}$, $\overrightarrow{BC}$ and $\overrightarrow{BD}$. The resultant voltage vector, $\vec{V} = \overrightarrow{V_R} + \overrightarrow{V_L} + \overrightarrow{V_{C+}} + \overrightarrow{V_{C-}}$ makes an angle φ with $\vec{I}$. Initially at a small frequency, let the state of the system be represented by the vector $\overrightarrow{OF}$ with $\varphi > 0$, indicating NC. At an increased value of frequency, let the system evolve to retain +ve capacitance with a final state: $\overrightarrow{OG}$ having $\varphi < 0$. Now, this transition can take place in two paths, associated with two completely different origin. The first one is the continuous dispersion from NCR to PCR, abundant in literature caused by continual effects of contact-injection & transport, slower transients, interference b/w M-W polarization and hopping conduction mechanisms, detrapping of charge-carriers etc. Here φ gradually decreases from +ve to –ve regime crossing through the frequency-axis. These dispersions can be mathematically modelled as an L-C-R circuit, where the state of the system passes through a point (on the real axis); where the two competing effects exactly cancel each other out leaving a purely resistive element.

5.4.2 Consolidated Results and Explanation:
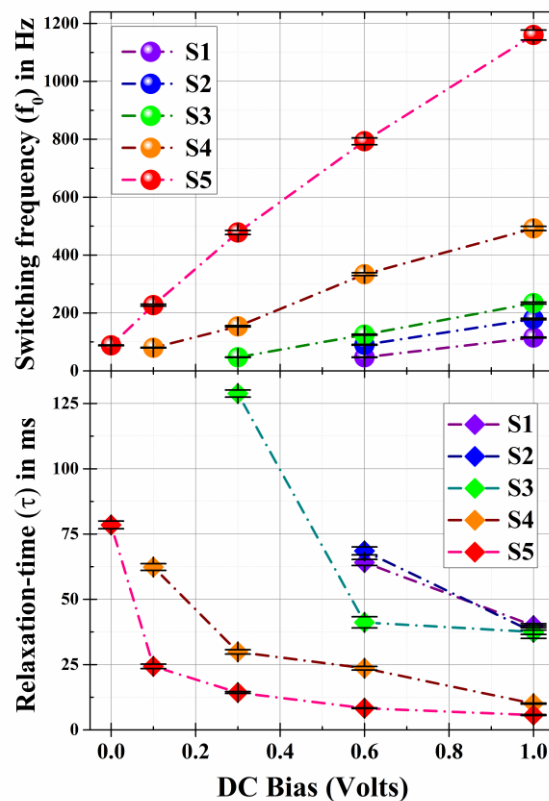
Fig 5.4: Consolidated results graph

To elaborate the second path a few concepts need to be introduced. An ideal dipole forms when two point-charges are separated by a small distance, possible for a mathematical lattice. In a real material, there are electron-clouds and charge-densities associated with a crystal structure, which have certain charge-centres (+ve/-ve). When two opposite charge-centres get separated by a finite distance, a 'light' dipole is formed. But, if the electron-cloud is sufficiently delocalized in case of more covalent bonds due to some point-defects or doping impurities, the associated dipoles get 'heavier', in a sense their effective length contracts reasonably with respect to the geometrical length; due to shifting of the electron-density towards the centre of the bond. For the same amount of external field, these 'heavy' dipoles are by definition less likely to get mobilized for sensing a reduced force/torque and thereby possesses higher electrical inertia. Hence these slow dipoles lag behind the AC signal and consequently originate NC. Now, as the frequency increases, it becomes more and more difficult to follow the input signal - resulting an increase in φ and at a limitting condition, $\varphi \to +90°, \tan \varphi \to \infty$. Eventually, further increase in frequency makes the system go beyond $\varphi = +90°$ and crossing a divergence (indicates an infinte discontinuity in C and loss-

maxima); ends up at $\varphi = -90°$ and finally settles to an acute negative φ. Basically, these heavy dipoles fail to achieve frequency-dependent dielectric saturation, as suggested by Richert and eventually encounters a switching to reach so. In this case, there is no such point in the evolution-trajectory of the system, in which it behaves like a pure resistor and here a switching takes place between NCR and PCR via a transient at a characteristic frequency i.e., the switching frequency (f_0). To recognize, the physical mechanism behind this mathematical model, we can describe the nature of the dipoles. The so-called 'light' dipoles being empowered by the high frequency of the alternating signal in presence of detrapped/injected carriers start eventually following up the input sweep and transit to NCR; whereas the slow and heavy dipoles lag further and further and consequently consumes an energy E_{flip} $(\sim f_0)$ to pursue a complete flip to get into PCR. Hence, the switching-frequency (f_0) is a measure of the flipping energy required for the mobilization of the 'heavy' dipoles and relaxation-time (τ) is a measure of the flipping-kinetics. Using this model, the variation of f_0 and τ with DC bias and particle-size can be explained as follows.

Sl. No.	Observations		Explanation
	Cause	Effect	
1	Increase in DC bias	f_0 increases.	At higher bias field, the dipoles get stiffened to its direction and show higher tolerance against the ac sweeps, hence require larger energy to flip around.
2		τ decreases.	At higher voltage, dipoles – a construction of charges acquire higher potential energy, which helps to speed up the flipping kinetics, and consequently the net flipping-time $(\approx 2\tau)$ decreases.
3	Decrease in particle-size	f_0 increases.	With decreasing grain-size, resistivity generally increases in semiconducting materials due to enhanced effect of grain-boundaries. A highly resistive sample is less likely to respond to a small external field, due to the faster voltage-drop. Hence, to flip the dipoles, a larger energy needs to be supplied.
4		τ and FWHM of loss-peaks decrease.	In a domain, the 'heavy' dipoles form their own mean field with a default orientation having optimized energy; modulatable by applied DC bias. The flipping kinetics basically compete with the mean field inside and try to reorient the associated dipoles. With a smaller domain-size, the mean-field effect weakens gradually and hence an external field can regulate faster the assembly of dipoles.

5.5. Conclusions:

Actually, the Type-I NC corresponds to non-Debye response of the associated samples, as continuous increment in charge-carriers due to contact-injection or detrapping violates the fundamental assumption of non-interacting dipoles. Hence, none of the updated models given by Cole, Davison, Harvriliak and Negami also fit to these observations. On the contrary, for Type-II NC, the relaxation-dynamics cease only at the time of dipole-flipping. Before and after this reversal, the dipoles relax the way suggested by Debye. Hence, in the low-frequency regime, due to a stable value of NC, these materials can be implemented as thin films in MOSFET devices for matching the +ve capacitance of normal dielectric oxides and thereby exploring new paradigms beyond the Boltzman tyranny on subthreshold swing.

5.6.References:

1. P. J. Walsh, R. Vogel, and E. J. Evans, Phys. Rev. 178, 1274(1969).

2. R. Vogel and P. J. Walsh, Appl. Phys. Lett. 14, 216 (1969).

3. J. Shulman, Y. Y. Xue, S. Tsui, F. Chen, and C. W. Chu, Phys. Rev. B 80,134202 (2009).

4. J. Shulman, S. Tsui, F. Chen, Y. Y. Xue, and C. W. Chu, Appl. Phys. Lett.90, 032902 (2007).

5. A. G. U. Perera, W. Z. Shen, M. Ershov, H. C. Liu, M. Buchanan, and W.J. Schaff, Appl. Phys. Lett. 74, 3167 (1999).6. C. D. Wang, C. Y. Zhu, G. Y. Zhang, J. Shen, and L. Li, IEEE Trans.Electron Devices 50, 1145 (2003).

7. C. Y. Zhu, L. F. Feng, C. D. Wang, H. X. Cong, G. Y. Zhang, Z. J. Yang,and Z. Z. Chen, Solid-State Electron. 53, 324 (2009).

8. E. Ehrenfreund, C. Lungenschmied, G. Dennler, H. Neugebauer, and N. S.Sariciftci, Appl. Phys. Lett. 91, 012112 (2007).

9. J. Bisquert, G. G. Belmonte, A. Pitarch, and H. J. Bolink, Chem. Phys.Lett. 422, 184 (2006).

10. M. Ershov, H. C. Liu, L. Li, M. Buchanan, Z. R. Wasilewski, and V.Ryzhii, Appl. Phys. Lett. 70, 1828 (1997).

11. C. C. Wang, G. Z. Liu, M. He, and H. B. Lu, Appl. Phys. Lett. 92, 052905(2008).

12. M. Ting, R. dos Reis, M. Jaquez, O. D. Dubon, S. S. Mao, K. M. Yu, andW. Walukiewicz, Appl. Phys. Lett. 106, 092101 (2015).

13.N. Mazumder, D. Sen, U. K. Ghorai, R. Roy, S. Saha, N. S. Das, and K. K.Chattopadhyay, J. Phys. Chem. Lett. 4, 3539 (2013).

14. Q. J. Liu, N. C. Zhang, F. S. Liu, and Z. T. Liu, Phys. Status Solidi B 251,1630 (2014).

15. K. Tang, S. Gu, K. Wu, S. Zhu, J. Ye, R. Zhang, and Y. Zheng, Appl.Phys. Lett. 96, 242101 (2010).

16. B. Y. Geng, G. Z. Wang, Z. Jiang, T. Xie, S. H. Sun, G. W. Meng, and L.D. Zhang, Appl. Phys. Lett. 82, 4791 (2003).

CHAPTER 6:

CONCLUSION

6.1 Grand conclusion:

In my thesis, an attempt has been made to interweave the results of my work's experimental observations with the help of theoretical explanation. The negative capacitance observed is obtained in milifarads (mF). The NC observed for all the samples have been investigated with different parameters and explained.

A new model was proposed and developed with the notion of 'heavy' dipoles, which is capable of explaining all the observations related to negative capacitive switching. The proposed modification to universal Debye relaxation before and after the switching can fit the experimental data emphasizing the dynamics of the slow & covalent dipoles, in the immediate vicinity of the total flipping of the dipoles, indicated by the loss-peaks mathematically alike to Delta functions. The stable NC dispersion below the switching frequency can be useful in building up MOSFETS to match the +ve capacitance of the dielectric oxide layer to go beyond the Boltzman tyranny on 60 mV/decade limit of subthreshold swing.

6.2 FUTURE SCOPES:

Negative capacitance is an innovative emerging research field in recent times and has potential applications. The future scope of this thesis includes certain modifications to pave the way for further improvements and applications listed below :

- ✓ Our study points to a novel scope for generating negative capacitance in a non-stoichiometric half-metallic iron oxide, which constitute a significant portion of contemporary electronics in terms of photovoltaics.

- ✓ These size-modulated nanoparticles can be used in modern integrated circuits, consisting of billions of semiconductor components, to remove the heat effectively which is generated during information processing. In other words, to reduce heat generation or self-heating in the ICs these materials with negative capacitance effect are useful.

- ✓ It can be used in transistors as they require lower operating voltages and to reduce transistors' increasing power dissipation and heat generation.

Fundamental aspects of NC as well as device applications can be triggered upon further experimental venture.